

Optical Engineering

OpticalEngineering.SPIEDigitalLibrary.org

Multiparameter fiber-optic sensors: a review

Simon Pevec
Denis Donlagic

Multiparameter fiber-optic sensors: a review

Simon Pevec and Denis Donlagić*

University of Maribor, Faculty of Electrical Engineering and Computer Science, Maribor, Slovenia

Abstract. Needs for sensor miniaturization, versatile sensing solutions, and improved measurements' performances in difficult operating environments have recently driven considerable research in optical fiber sensor for multiparameter measurements. Multiparameter sensors not only enable new sensors' functionalities, but can also improve achievable measurement performances for some frequently measured parameters considerably. This study provides a review of work in the field of miniature fiber-optic sensors that allows independent and simultaneous measurements of two or more different physical or chemical parameters. Sensor designs and corresponding signal processing schemes are reviewed and compared. © 2019 Society of Photo-Optical Instrumentation Engineers (SPIE) [DOI: [10.1117/1.OE.58.7.072009](https://doi.org/10.1117/1.OE.58.7.072009)]

Keywords: multiparameter sensing; fiber-optic sensors; design and fabrication; temperature; pressure; strain; refractive index; curvature; bending; force; Fabry–Perot; fiber Bragg gratings; Mach–Zehnder interferometer; Michelson interferometer; surface plasmon resonance.

Paper 181705SSV received Nov. 29, 2018; accepted for publication Feb. 14, 2019; published online Mar. 6, 2019.

1 Introduction

Optical fiber sensors have been the topic of intense research for many years. Recent progress in performance and cost reduction of passive optical fibers devices and active opto-electronics components, driven by telecom and other photonics-related fields, has led to firmer penetration of fiber-optic sensors into various industrial, medical, environmental, power, defense, and other applications. Reasons for introduction of fiber-optic sensors' solutions into new application fields are usually associated with one or more fiber-optic sensors' attributes that are usually not available with other (electrical/electronic) sensing systems, such as dielectric sensor design, immunity to electromagnetic interference, harsh environment compatibility (high temperatures, chemical resistance, and radiation environment compatibility), multiplexing, and distributed sensing capability and cylindrical geometry. In addition to these well-known properties, fiber-optic sensors, however, also provide interesting opportunities for miniaturization and design of sensors that can measure independently and simultaneously more than one physical or chemical parameter. These possibilities were explored more intensively only recently, and it is the aim of this article to review these approaches. Multiparameter sensors require appropriate signal interrogation approaches, which are also discussed briefly within this review. The current review, however, does not cover multiplexed sensors that are composed of multiple individual sensors aimed for measurement of different parameters. Although sometimes the difference between multiplexed sensors aimed for measurements of different parameters and multiparameter sensors might not be clear, we focus in this review on sensors that are spatially confined, not separated by longer section(s) of fiber(s), and also miniature in size.

Compact size and multiparameter sensing capability might present an important evolution step in sensing systems for several reasons. Multiparameter sensing is often unavoidable in a process of acquiring desired information on a system state and/or performance. For example, refractive index (RI) of a liquid is usually measured with the aim of determining the liquid's composition. Most liquids are, however, highly temperature sensitive, and determination of RI by itself might not provide sufficient information on the characterized liquid composition, especially in environments with broad operational temperature ranges. Thus temperature must also be known to extract liquid composition from an RI measurement. This problem becomes more pronounced when higher measurement resolutions and accuracies are required, which demands very precise knowledge of the actual measured sample's RI and temperature. In a case like this, the quality of the temperature compensated measurement result (which is correlated to the liquid composition) depends not only on both RI and temperature sensing performances, but also on the spatial proximity of both sensors/sensing segments, as temperature gradients with the measured sample can quickly lead to significant measurement errors. To obtain meaningful RI data with resolution in the range of 10^{-6} refractive index unit (RIU), the temperature of the measured sample must be known with an accuracy of about 10 mK or better in the case of a typical liquid. In instances like this, a compact design of multiparameter sensor is unavoidable, especially when the sensor is used in less controlled temperature environments, which are often encountered in out of the laboratory applications.

In the first part of this review, we classify multiparameter sensors according to their principles of operation. This part also discusses associate signal and interrogation and processing techniques, which usually differ from those encountered in conventional single-parameter sensors. In the second part of the review, we classify multiparameter sensors according to sets/combinations of different parameters that can be measured simultaneously with respect to the principles of operation.

*Address all correspondence to Denis Donlagić, E-mail: denis.donlagic@um.si

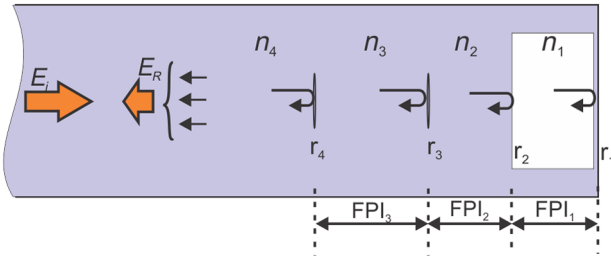


Fig. 1 Typical stacked multiparameter Fabry-Perot sensor.

2 Basic Designs and Principles of Operation of Multiparameter Fiber-optic Sensors

2.1 Multiparameter Sensors Based on Stacking of Fabry-Perot Interferometers

Fabry-Perot interferometers (FPIs) are especially suitable for a design of multiparameter fiber-optic sensors. There are several reasons for this: first, unlike fiber Bragg gratings (FBGs), FPIs can be used to sense directly a very broad span of different parameters, ranging from mechanical quantities, such as strain and pressure to different chemical sensing applications. Second, FPIs are mostly compact in dimensions and can be stacked one on the top of another to form a multiinterferometer system, shown in Fig. 1. Third, stacked FPIs can be interrogated very efficiently with low crosstalk by application of conventional optical spectrum interrogation methods. In the latter case, individual measurement FPIs must possess different optical path lengths.

Once the optical spectrum of the stacked FPI or any other multiple-interferometric sensor is acquired, there are several approaches that can be applied to extract individual interferometers' path length variations from the acquired spectrum. Among these, the matrix method is one of the most commonly encountered. In the matrix method,¹⁻⁷ an assumption is made that selected spectral features (usually preselected peaks or dips) positions within the spectrum are all linearly dependent on measured parameters, however, each selected feature with a different sensitivity to a particular parameter. Thus a set of linear equations (matrix) can be formed and solved for individual FPIs or other interferometers' length changes, representing individual measured parameter changes. For instance, when dealing with a two-parameter sensor for simultaneous measurement of pressure and temperature, as presented in Ref. 5, changes in selected and observed peaks positions in a back-reflected sensor's spectrum ($\Delta\lambda_1$ and $\Delta\lambda_2$) depend linearly and simultaneously on both measured parameters (pressure and temperature). Thus a set of two linear equations can be used to establish relations between selected peaks' position changes and changes in measured parameters:

$$\begin{aligned} \Delta\lambda_1 &= K_{P1} \cdot \Delta P + K_{T1} \cdot \Delta T \\ \Delta\lambda_2 &= K_{P2} \cdot \Delta P + K_{T2} \cdot \Delta T \end{aligned} \quad \text{or} \quad \begin{aligned} \begin{bmatrix} \Delta\lambda_1 \\ \Delta\lambda_2 \end{bmatrix} &= \begin{bmatrix} K_{P1} & K_{T1} \\ K_{P2} & K_{T2} \end{bmatrix} \begin{bmatrix} \Delta P \\ \Delta T \end{bmatrix} = K \begin{bmatrix} \Delta P \\ \Delta T \end{bmatrix}, \end{aligned} \quad (1)$$

where K_{P1} represents a sensitivity coefficient that relates the change of the first selected spectral peak position $\Delta\lambda_1$ to the pressure change. Similarly, K_{P2} represents a sensitivity

coefficient that relates the change of the second selected spectral peak position $\Delta\lambda_2$ to the pressure change, while K_{T1} and K_{T2} relate the first- and the second-peak position changes due to the temperature change. These coefficients can be conveniently grouped further in a sensitivity matrix K , which relates and describes in full the shift of spectral peaks with measured parameters. Rearranging Eq. (1) by calculating the inverse matrix of K provides the next final matrix form, which enables individual calculation of temperature and pressure changes when the changes in peak positions $\Delta\lambda_1$ and $\Delta\lambda_2$ are known:

$$\begin{bmatrix} \Delta T \\ \Delta P \end{bmatrix} = \frac{1}{\det K} \begin{bmatrix} K_{T1} & -K_{T2} \\ -K_{P1} & K_{P2} \end{bmatrix} \begin{bmatrix} \Delta\lambda_1 \\ \Delta\lambda_2 \end{bmatrix}. \quad (2)$$

Thus an arbitrary two-, or more than two, parameter system can be described by the matrix approach described above, as long as the determinant of matrix K is nonzero (i.e., individual observed features must possess different sensitivities to individual parameters).

The matrix method is applicable not only to FPIs, but in general, to any sensor configuration which involves multiple measurable optical parameters/features (e.g., interference or grating spectral peaks or valley, phases, and intensities) that depend on multiple measured physical or other parameters (temperature, strain, pressures, RI, etc.). Thus we will refer frequently to the matrix method throughout this review.

Another highly efficient method that can yield very low crosstalk among measured parameters and high-measurement resolution is based on inverse discrete Fourier transform (IDFT).⁸ This method is applicable to low-finesse FPI (which are usually encountered in fiber sensors) that possess cosines back-reflected spectral characteristics. The principle is certainly also applicable to the other two-beam multiple/stacked interferometers. A period of an interference cosine spectral fringe in a spectral characteristic corresponds to the FPI's free spectral range (FSR), i.e., $FSR = c/2nd$, where c presents speed of light in vacuum, n is the RI, and d is the distance between two reflective surfaces of FPI resonator. Thus stacking of multiple low-finesse interferometers (like low-finesse FPIs) with different lengths yields a back-reflected spectrum containing multiple harmonic components, which can be separated straightforwardly by the application of discrete Fourier transformation (strictly speaking, IDFT, as we perform transformation on the optical spectrum, which yields values that belong to a time domain). IDFT performed on a multiple interferometer/cavity system spectrum yields an amplitude IDFT, which has multiple local peaks. Each local peak in IDFT represents a round trip time of flight between a pair of semireflective mirrors present in the stacked FPI system. While observation of individual peaks in amplitude IDFT can provide means for direct and absolute interferometer length measurements, this approach is limited, due to the limited resolution of IDFT, which is determined by the spectral bandwidth of the interrogation system (to get a high resolution, a spectrum over a very broad wavelength range shall be acquired). However, tracking of the phase(s) of the IDFT components that correspond to the peak values in the absolute IDFT allows for very efficient and high-resolution tracking of the interferometer's length changes (resonators' length changes in miniature FPIs are usually small, and phase tracking proves to be an efficient

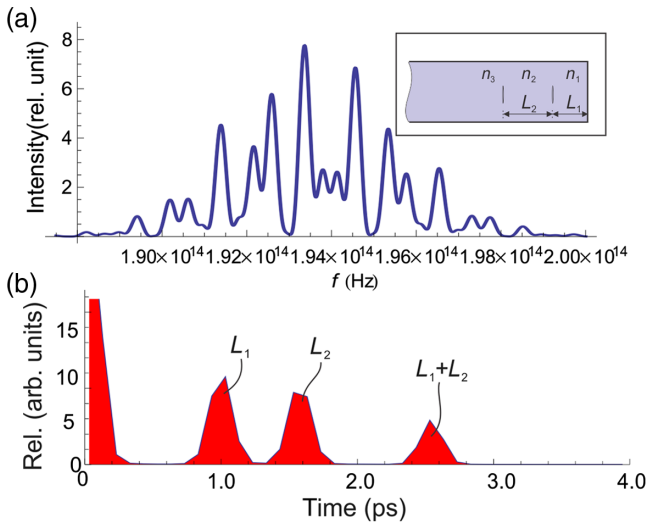


Fig. 2 (a) Experimental measured optical back reflected spectrum and (b) its IDFT for a dual (145- and 230- μm long) FPI system.

way for FPI multiparameter sensor interrogation). An example of this approach is provided below. Figure 2 shows a back-reflected optical spectrum of a sensor consisting of two FPIs as shown in Fig. 2(a) insert.

The spectrum is expressed in a way that the x axis represents optical frequency (this is necessary to perform IDFT properly). The first and the second FPIs are 145- and 230- μm long. The absolute value of IDFT of the acquired optical spectrum is shown in Fig. 2(b). Note that the x axis is now in time units. Each peak in the absolute IDFT is generated by a pair of semireflective mirrors, and the position of each peak in the absolute IDFT represents a round-trip time of flight among a mirror pair. Thus by multiplying the x axis by $c/2$ yields the system’s resonator lengths. Note that two stacked FPIs, which are defined by three semireflective mirrors, yields an absolute IDFT with three local peaks, as three possible interference paths are formed: mirror 1 and mirror 2 define the first FPI, mirror 2 and mirror 3 define the second FPI, and mirror 1 and mirror 3 define the third interference path. To observe small variations of any of these paths, one needs to calculate and track the phases [$\phi = \arctan(\text{Im}/\text{Re})$] of complex IDFT components, in which peaks occur in the absolute IDFT. This IDFT-based technique allows for a very efficient and crosstalk-free separation of individual spectral components within an acquired optical spectrum generated

by more than one FPI. Another important property of this method is that the method utilizes the entire set of acquired spectral data points to calculate the interference fringe position in the optical frequency domain. Unlike the commonly used methods for spectral shift tracking of sensors’ characteristics, which rely on a single-local peak (or dip) tracking, and which take advantage of only a limited set of local spectral data points around the tracked peak, IDFT utilizes in full the entire available spectral data acquired by the signal interrogator. This is reflected in a low-output measurement noise, which is especially beneficial in high-resolution measurement systems.⁹

Multiparameter Fabry–Perot sensors are frequently found as sensors for simultaneous pressure and temperature measurements. Pressure and temperature are also two parameters that need to be measured simultaneously in a wide spectrum of very different applications, ranging from process industry to medical uses. Unlike most other common fiber sensing technologies [FBGs and Mach–Zehnder interferometers (MZIs)], Fabry–Perot sensors are well-suited for pressure measurements, due to their ability to directly measure a deflection of a pressure-sensitive diaphragm positioned in front of an optical fiber. Stacking of two FPIs that are selectively sensitive to either pressure or temperature is often used to design sensors for simultaneous measuring of temperature and pressure.^{3–7,10–12} Most frequent designs utilize a stack of two FPIs at the tip of a fiber, where the first FPI is made from a temperature-dependent waveguide [e.g., single mode fiber (SMF), other waveguide, or temperature-sensitive layer], while the second FPI is usually realized as a cavity, which is defined by a reference surface and a flexible diaphragm. The latter can be made out of different materials and using different manufacturing techniques.^{3,4,7,10–12} Very compact and robust sensors made entirely from silica glass based on this approach are described.^{4,11} In both cases, a section of SMF placed in-between two semireflective in-fiber mirrors, is used to make the temperature-sensitive FPI. The pressure-sensitive FPI is made by fusion-splicing a short section of fiber to a lead-in fiber that contains a micromachined cavity on its tip. The short-spliced fiber segment is thinned further to form a flexible pressure-sensitive diaphragm [Fig. 3(a)]. The selective etching process is used to form the cavity,¹¹ while in Ref. 4, the cavity is made by femtosecond micromachining. A similar structure is also reported,¹² however, using different materials and process to create a pressure–temperature sensing FPI pair. In Ref. 12, the pressure sensing structure employs a

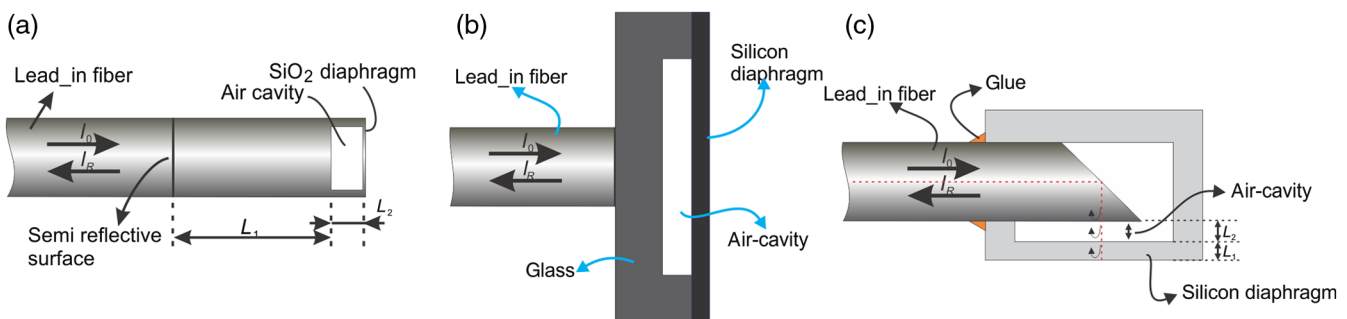


Fig. 3 Different pressure–temperature sensor designs: (a) All-fiber, all-silica design, (b) large silicon diaphragm attached to the fiber tip using MEMS technology, and (c) MEMS design includes polished fiber with 45-degree angled end-face and silicon diaphragm.

polymer/metal composite diaphragm with high-pressure sensitivity. The temperature sensing is achieved using an intrinsic silica/polymer FP cavity that is adjacent to the pressure-sensing cavity. Another approach to the design of combined pressure–temperature sensors is to use a miniature MEMS chip that is attached to the fiber tip. Examples of these approaches can be found in Refs. 3 and 10. In these approaches, a suitable silicon MEMS chip is created and glued onto the tip of a fiber [Fig. 1(b)] or onto a ferula containing optical fiber. The MEMS chip as described in Ref. 7 is a three-layer structure made from a silicon substrate, Pyrex glass (with etched cavity), and a silicon diaphragm, as illustrated in Fig. 1(c). The silicon substrate acts in this case as a temperature sensing FPI, while the cavity created between the substrate and diaphragm as a pressure-sensitive part. In a design presented in Ref. 7, Pang et al. proposed a dual-cavity configuration consisting of a polished fiber with 45-deg angled end face, silicon diaphragm, and a silicon housing. In this case, the sensing cavity axis is perpendicular to the fiber axis, which allows for design of a larger and thicker silicon diaphragm. In this case, a sufficiently thick diaphragm also acts as a temperature sensing FPI.

All the aforementioned sensors use FPI pairs with distinctive lengths that generate distinctive interference fringe frequencies in the back-reflected spectrum. Individual peaks in the spectrum, or better phases of characteristics’ spectral components, can then be tracked to resolve pressure and temperature unambiguously, as already described in the signal interrogation section aforementioned. In some instances,¹⁰ different wavelengths are used to obtain responses from different FPI surfaces (silicon absorbs wavelengths below 1000 nm strongly, but is quite transparent at 1550 nm, which allows for selective readout of individual cavities). Furthermore, sometimes a total back-reflected light¹⁰ rather spectral signature is observed to determine at least one of the measured parameters. Another approach to combined temperature–pressure sensing is based on an indirect pressure sensing method, where the RI of the gas is measured and correlated to the pressure. This eliminates limitations associated with diaphragm nonlinearity and drifts, but limits use of sensors like this to gas pressure sensing, complicates temperature compensation, requires calibration to a specific gas, and makes the sensor prone to contamination. Sensors like this include a temperature-sensing segment combined by an open path FP cavity.^{5,6} In Ref. 5, a short segment of capillary is fusion-spliced to the fiber tip. Then a glass microsphere is inserted into the capillary to define two FPIs, one sensitive to temperature (defined by the diameter of the glass microsphere), and the other predominantly to RI/pressure (FPI defined by fiber end and microsphere). Another example of this indirect method, pressure–temperature sensor is described in Ref. 6. It consists of two, stacked open path FPIs/cavities; one cavity is made from a capillary, and the second FPI from a phonics crystal fiber (PCF). Air holes in the PCF cladding area are used as gas “tunnels” to the capillary-based cavity. Consequently, both FPIs are sensitive to temperature and pressure, while these sensitivities differ and allow for pressure and temperature separation using the matrix method approach.

Sensors combining parameters other than pressure and temperature are also feasible by FPI stacking. A sensor for simultaneous sensing of pressure and RI is reported in

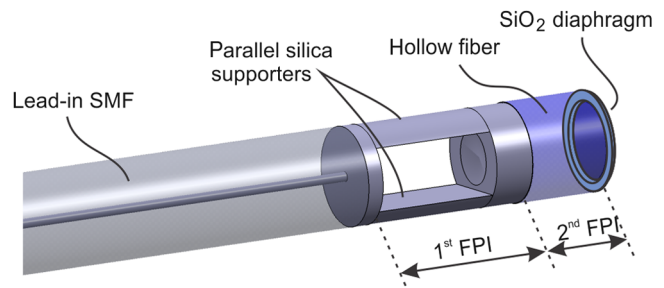


Fig. 4 Pressure and RI sensor.

Ref. 2. This design also utilizes two stacked FPIs; the first FPI is an open path microcell for RI sensing, whereas the second FPI is an air cavity with all-silica diaphragm for pressure sensing, as shown in Fig. 4.

FPIs can also be found in applications for sensing of various other multiple parameters. Simultaneous strain and temperature sensing by stacking two FPIs was reported in Refs. 1 and 13. These two sensor examples are both composed of two FPI segments that possess different temperatures and strain sensitivities, allowing for strain and temperature determination using the matrix method. In Ref. 1, a short-glass capillary is fusion spliced in-between two SMFs to form the first FPI segment, whereas the second sensing FPI segment is composed of a short section of SMF with semireflective surfaces on both sides of this segment as shown in Fig. 5.

In Ref. 13, the first FPI sensing segment is composed of a short-air-cavity, created by laser machining, whereas the second FPI segment is the same as in Ref. 1. Another FPI-based multiparameter sensor for measurement of mechanical parameters is reported in Ref. 14 and allows for simultaneous measurement of strain and directional bending. The design utilizes a dual-side-hole fiber, spliced in-between a 7-core fiber and multimode fiber to form an FPI sensing pair. Because of the different directional bending sensitivities and almost identical strain sensitivities of both FPIs, the discrimination of both parameters (using the matrix method) is feasible.

FPIs also provide opportunities to design very high-resolution sensors for simultaneous measurements of RI and temperature. Examples of sensors like this are described in Refs. 15 and 16. Both sensors’ designs are based on a combination of an in-fiber, all-SiO₂ FPI, which is sensitive only to temperature and an open path micromachined microcell (Fig. 6). The microcell has low-intrinsic sensitivity to temperature, however, responds strongly to RI change. Proper temperature compensation methods are presented in both references (using an integrated temperature sensor), which allowed for determination of RI change corresponding

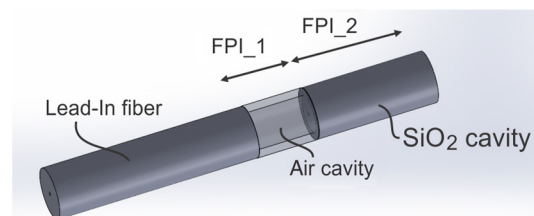


Fig. 5 Strain and temperature sensor.

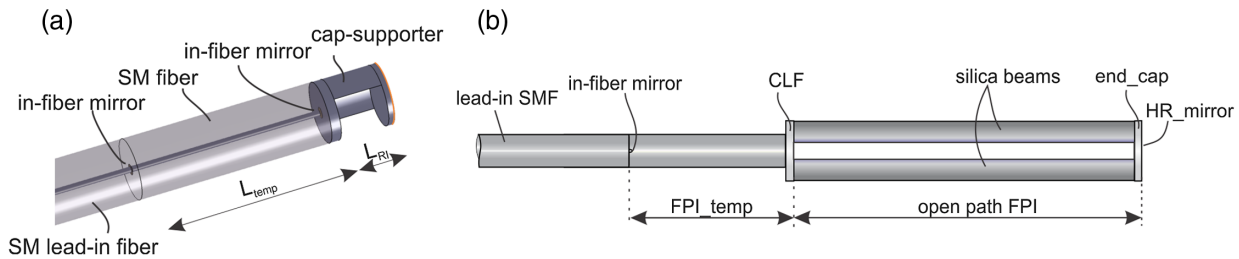


Fig. 6 RI and temperature sensors: (a) for liquid sensing applications and (b) for gas sensing applications.

purely to the fluid’s/gas’s composition change with resolution as high as 2×10^{-7} and 5×10^{-9} of RIU.

Cascaded FPIs also provide opportunities for design of relative humidity and temperature sensors. In Ref. 17, a humid-sensitive FPI is formed by a thin micromachined microwire covered by a porous layer of SiO_2 , whereas the temperature sensing FPI is made from a segment of a standard single-mode fiber, as already described in the sensor cases aforementioned, such as shown in Fig. 7.

Finally, stacking of multiple FPIs was also demonstrated to measure up to four different parameters simultaneously: thermal conductivity, pressure, RI, and temperature.¹⁸ The sensor utilizes three different FPIs stacked on the tip of a lead optical fiber as shown in Fig. 8. The first FPI is made of a glass capillary and a flexible silica diaphragm for pressure sensing. The second FPI is a long open path all-silica microcell, which allows for free access of the surrounding gas into the cavity and provides RI sensing capability. A short section of vanadium-doped fiber defines the third FPI, which performs two functions: temperature sensing and thermal conductivity measurement. Thermal conductivity measurement is achieved by active laser heating

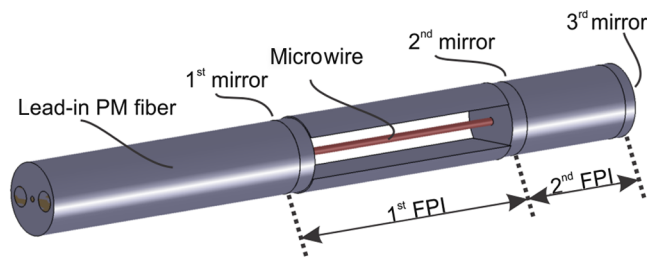


Fig. 7 Relative humidity and temperature sensor.

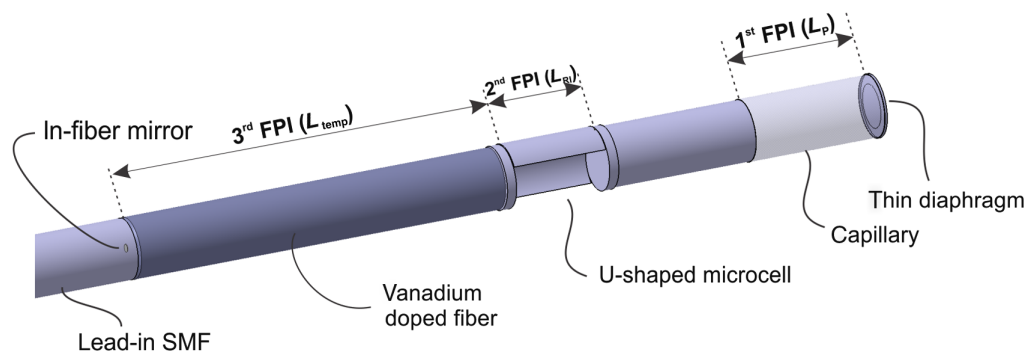


Fig. 8 Four-parameter sensor for simultaneous measurements of thermal conductivity, pressure, RI, and temperature.

of the vanadium fiber, which absorbs short wavelengths selectively (e.g., 980 nm), but is relatively transparent at longer wavelength range (e.g., 1550 nm). The change in temperature of this segment during application of heating power allows for determination of the surrounding fluid’s thermal conductivity.

2.2 Multiparameter Sensors Based on Mach-Zehnder and Michelson in-Fiber Interferometers

In-fiber MZIs and, less frequently, Michelson interferometers (MI) are of particular interest for building multiparameter sensors, as they provide relatively straightforward and versatile ways to implement different cascaded interferometric configurations. Individual MZIs and/or MIs are usually formed by local coupling of two (sometimes more than two) modes within the fiber. Depending on the sensed-parameter, interference of fundamental and higher order mode(s) or interference of fundamental and fibers’ cladding mode(s) are employed most frequently. There are different ways in which controlled modal coupling can be obtained, but in general, it can be classed into the following groups:

- a. *Splicing of fibers with dissimilar modal fields.*^{19–25} Fibers with dissimilar modal fields are spliced together to facilitate the transfer of optical power from one mode of the lead fiber to two or more modes of the sensing fiber. Typical examples representing this group include sensor structures that utilize splices between single-mode and step-index few-mode or multimode fibers or core-less fibers, as shown in Fig. 9.
- b. *Offsetting fibers.*^{26,27} In this case, fibers are offset from the longitudinal axis and usually spliced to form a solid structure. For example, by offset-splicing

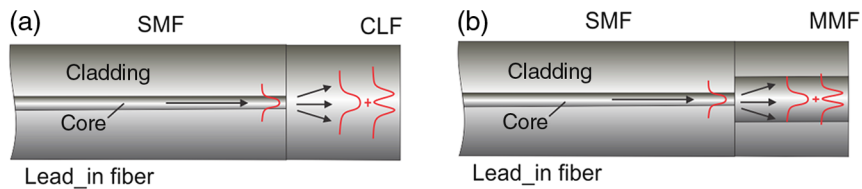


Fig. 9 Typical examples for splicing fibers with dissimilar modal fields: (a) SMF-CLF (coreless fiber) and (b) SMF-MMF.

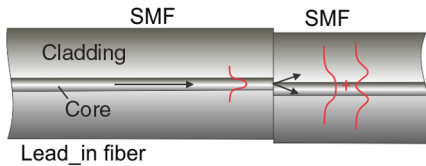


Fig. 10 Offset splicing of SMF: core and cladding modes are excited.

of two single-mode fibers, both fundamental and cladding modes are excited in a sensing fiber. This approach is used frequently to design sensors for measurements of RI (Fig. 10).^{26,27}

- c. *Abrupt (nonadiabatic) tapers.*^{28–32} Short-high-pitch (nonadiabatic) tapers can act as effective mode coupling events that can couple guided and cladding modes or different guided modes within few or multi-mode waveguides (Fig. 11).
- d. *Other local perturbations.*^{33–37} Microbends or similar local perturbations in fiber geometry can also act as mode coupling events and can be used efficiently to build MZI or MI (Fig. 12).

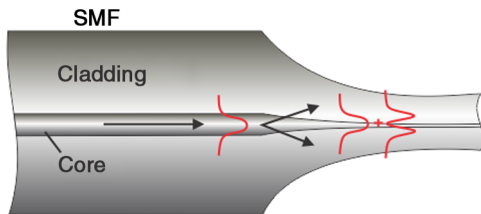


Fig. 11 Abrupt taper.

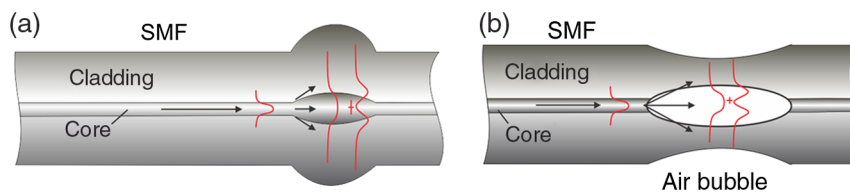


Fig. 12 Typical examples of local perturbations: (a) with microsphere and (b) coupling with air-bubble.

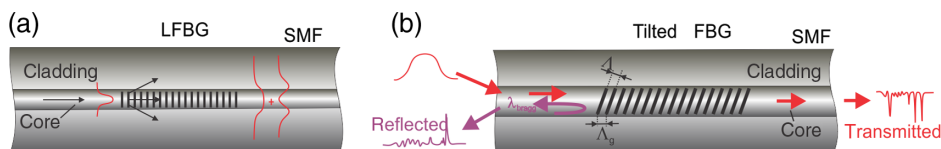


Fig. 13 Utilization of: (a) LPFBG and (b) tilted FBG.

- e. Utilization of long-period³⁸ or tilted long-period Bragg gratings, which act directly as localized coupling events among target modes or modal groups. Generalized examples of these approaches are shown in Fig. 13.

Combinations of the different coupling principles described above are also possible and actually encountered frequently within the same multiparameter fiber sensors.

Signal interrogation in these types of sensor usually utilizes spectral interrogation in conjunction with already described matrix method, where characteristics' peaks/dips with different sensitivities to individual measured parameters are tracked in a back-reflected optical spectrum.

MZIs are encountered most frequently in sensors for simultaneous measurement of RI and temperature. The two most often reported approaches utilize either a single MZI^{23,24,27,29,30,33–37} or a cascading of two MZIs.^{19–21,26,31,38}

- a. *Using a single MZI for temperature and RI sensing.* The single MZI can be used to measure RI and temperature simultaneously by creating an MZI that utilizes interference of multiple (three or more) modes in a waveguide section that provide evanescent interaction with the surrounding medium for one or more of the involved modes. Since the phase constants of those modes that reach out into the surrounding medium, depend on the medium's RI, any change in RI modulates spectral response of the sensor in a distinctive way. For example, in a transmission spectrum, characteristic features (e.g., peaks/dips) appear that belong predominantly to the interference of particular modal pairs. Since the phase constants of individual modes exhibit different dependences on

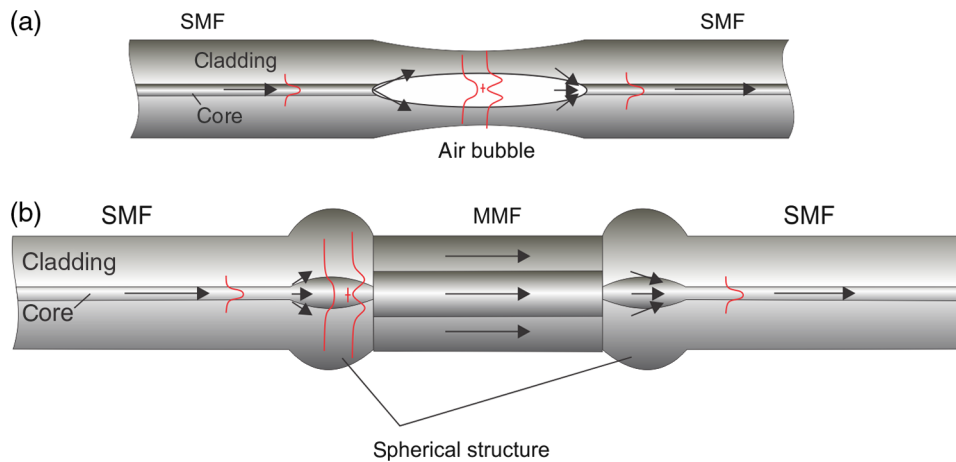


Fig. 14 Temperature and RI sensors based on MZI: (a) with air-bubble perturbation and (b) with spherical structure perturbation.

the surrounding RI and temperature, sensitivities of these distinctive spectral features (peaks/dips), possess different sensitivities to RI and temperature. For small changes in temperature and RI, the matrix method can be used to resolve temperature and RI independently from each other. Even more efficient separation among individual interference paths in such multimode MZI (or MIs) can be obtained if the IDFT processing method is applied (described in Sec. 2.1).

Examples of the approach described already are used in Refs. 23, 29, 30, 33–36, and 39. These designs all use interference among a path/mode that is protected from the surrounding RI influence (core mode or intracavity mode), and different cladding modes that are RI dependent (but to a different extent) as shown in Fig. 14. The main differences among the described principles are in designs that lead to proper mode coupling in fibers that are used to create multimode MZI.

References 27 and 37 represent somehow a special example of multimode MZI, where the interference among cladding modes and LP modes of the highly birefringent (HB) fiber is used to obtain different RI and temperature responses. Another example of a single MZI configuration for simultaneous RI and temperature measurement is presented in Ref. 24, where spectral shift and amplitude of a selected peak/dip are correlated to the RI and temperature (here, a peak/dip amplitude modulation is used in addition to spectral peak position to determine RI and temperature).

- b. *Cascading of MZIs for temperature and RI sensing.* When two MZIs are cascaded, one is usually made sensitive to temperature, and the other to RI and temperature (while not desired, temperature sensitivity of

RI sensing MZI is usually unavoidable due to the fiber's and fluid's intrinsic temperature sensitivity).

In Ref. 20, a single-mode fiber is used to excite modes in a short section of multimode fiber, which acts as a temperature sensing MZI, while the RI-sensitive section is made by an abrupt short taper (Fig. 15), made of single-mode fiber preceding the multimode fiber section. (Thus multiple modes are excited in the tapered section.)

An elongated in-fiber bubble is formed in Ref. 31 to redirect part of the light propagating within the core of a single-mode fiber into the cladding and provide an RI-sensitive MZI. This structure is followed by a short piece of microstructured fiber that supports several modes, and interference among those modes provides the desired temperature sensing function. In Ref. 21, a temperature insensitive Interferometer is created by exciting higher-order modes in a short section of multimode fiber, while the RI sensing interferometer is formed by excitation of cladding modes in a short section of a single-mode fiber [Fig. 16(b)]. Similarly, the combination of a short core-less fiber section and a section of multimode fiber¹⁹ can be used to create an RI-temperature-sensitive interferometer pair [Fig. 16(a)]. A short-multicore fiber section combined with a multimode fiber was used [Fig. 16(c)] to create an RI-temperature sensing MZI pair.²⁶

The previously described principles include quite different designs of both cascaded MZIs, which often leads to relatively complex assembly procedures. However, nearly identical MZI pairs can also be designed in a way to provide an RI-temperature sensing capability. An example of a configuration like this is presented in Ref. 38, where three long-period fiber Bragg gratings (LPFBGs) are used to create two MZIs, however, LPFBG periods are selected in a way to excite cladding modes with different modal orders, which

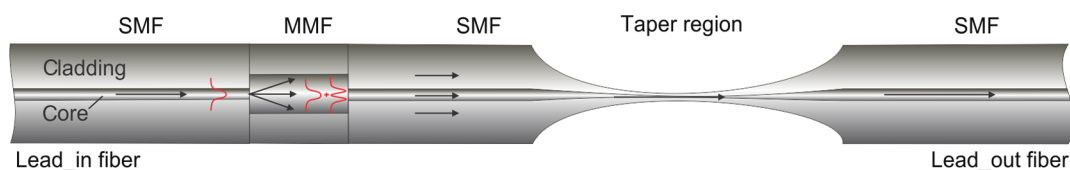


Fig. 15 Temperature and RI sensors based on SMF-MMF-SMF elongated with a taper region.

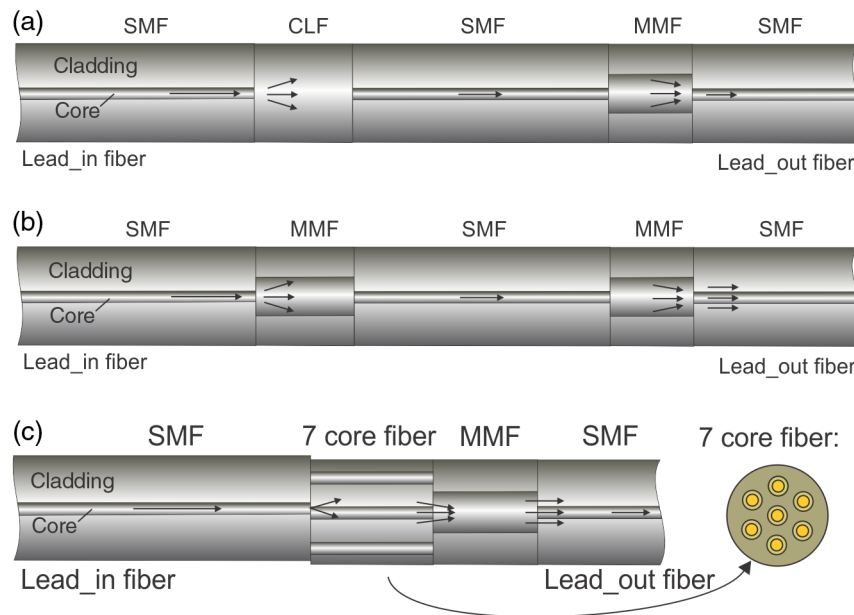


Fig. 16 Temperature and RI sensors based on different MZI configurations: all based on splicing fibers with dissimilar modal fields: (a) between SMF-CLF and MMF-SMF, (b) between SMF-MMF, and (c) between SMF-7 core fiber and MMF-SMF.

leads to different sensitivities of both MZIs to temperature and RI. The matrix method is used to resolve both parameters independently from one another.

MZIs can also be configured to measure simultaneously parameters other than RI and temperature. For example, MZIs were reported in dual-parameter sensors for strain and temperature measurements.^{22,40} In Ref. 40, a single MZI is created by “sandwiching” a straight section of a polarization maintaining fiber between two peanut mode coupling structures and standard SMFs, as illustrated in Fig. 17(a). This creates two distinctive modal interference patterns and similarly as in the case of single MZIs for RI-temperature sensing, two peaks/dips in the spectrum are selected and their shifts correlated to strain and temperature using the matrix method. Cascading of two MZIs can also be used to yield in combined strain-temperature sensors. In this

case, MZIs exhibit different sensitivities to temperature and strain, and their responses can be correlated to strain and temperature by employing the matrix method. An example of this approach is demonstrated in Ref. 22, where sections of two short, but different, multimode fibers are “sandwiched” in-between two lead single-mode fibers [Fig. 17(b)].

MZIs were also reported as dual-parameter sensors for curvature and temperature measurements. A single MZI configuration with lead SMF, a short hollow core (capillary) section, and two mode coupling sections on each side of the hollow core section were reported in Refs. 25 and 28. Simultaneous pressure and temperature sensing was also demonstrated successfully by an MZI that utilizes a single, short section of two-mode HB fiber.⁴¹ Here, external pressure and temperature modulate the spectral responses of the MZI

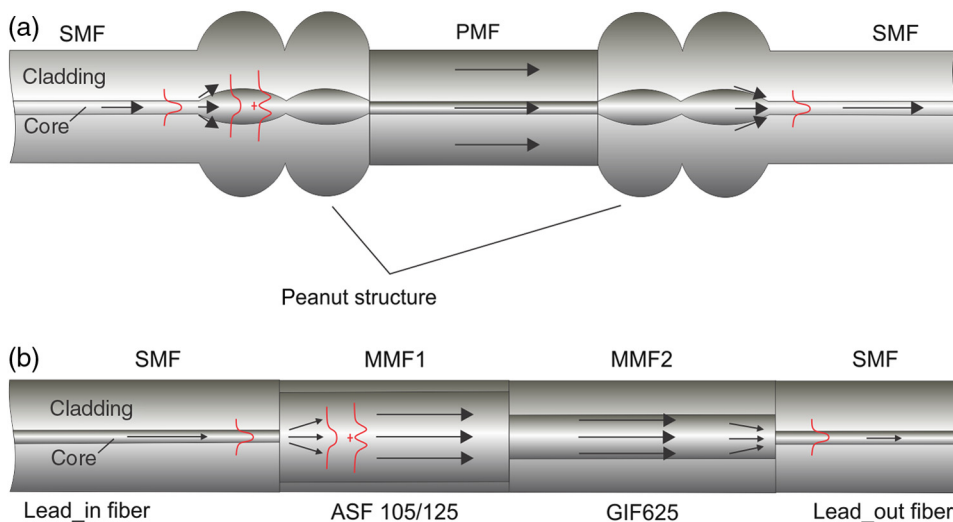


Fig. 17 Strain and temperature sensors based on different MZI configurations: (a) based on peanut structure and (b) based on splicing fibers with dissimilar modal fields.

in distinctive ways, which allows for reconstruction of temperature and strain.

MZIs were also demonstrated to measure three parameters simultaneously: RI, strain and temperature.^{32,42} Tapered bend-insensitive fiber-based MZI configuration is presented in Ref. 32. RI, temperature and axial strain parameters are measured for each outer-cladding mode. The authors use a peak wavelength shift and phase shift monitoring to fulfill matrices of the MZI to demonstrate simultaneous measurement of multiple environmental parameters. In Ref. 42, a single MZI was created out of a standard SMF using two symmetrical mode coupling events and an additional taper between both coupling events. Three distinctive spectral features (dips) were chosen in the transmitted spectrum and were correlated to strain, RI, and temperature using the matrix method.

2.3 Multiparameter Sensors Based on Combinations of MZI/Michelson Interferometers and FPIs

Combinations of Fabry–Perot and MZI/MI can also yield a variety of dual-parameter sensors. The potential benefit of such interferometer combination lay in the fact that the spectral responses of both interferometers can be made quite distinctive, which might yield easier and low-crosstalk separation of the measured parameters.

Combinations of FPI and MZI/MIs are reported for simultaneous RI and temperature measurements.^{43,44} In Ref. 43, two cascaded interferometers are presented: a 700- μm long in-fiber FPI for temperature measurements (formed by two in-fiber air gap mirrors), and an MI formed by inscribing an LPFBG at a distance of about 1.3 cm away from the fiber end, as shown in Fig. 18. The spectral response of the FPI is only temperature-dependent, whereas the spectral response of the MI shows both temperature and RI dependence.

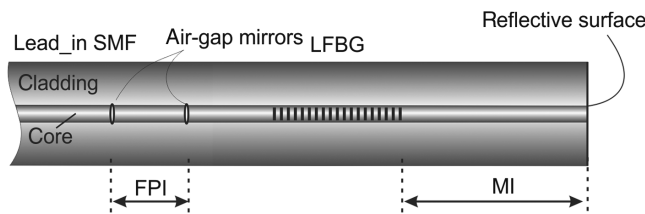


Fig. 18 Temperature and RI sensor.

An RI-temperature sensor was also created in a similar way in Ref. 44. Here the temperature-sensitive segment was created by a temperature-sensitive FPI cavity filled by alcohol, whereas RI sensing was achieved by forming an MZI using a hybrid hollow-core-PCF fiber section, in which both core and cladding modes are excited (Fig. 19).

Another example of an RI-temperature sensor was reported in Ref. 45, where the fibers at the output of an 2×2 coupler were shortened and trimmed to a short-length difference (of about 2 mm) to form a temperature-sensitive MI. Then one of the fibers at the coupler’s output port was further offset-spliced to a PCF, which forms an additional MI that is sensitive to the surrounding RI.

Simultaneous magnetic field and temperature sensing were also reported by combining an FPI with MZI.⁴⁶ The proposed approach is identical to the one reported in Ref. 44 except that the alcohol was replaced by magneto-optic fluid.⁴⁶

2.4 Multiparameter Sensors Based on FBGs and LPFBGs

FBGs provide many different ways to design multiparameter sensors. Bragg gratings are used essentially to induce coupling between two modes. The coupling occurs when the phase-matching condition is satisfied. This condition is given by

$$\beta_1 - \beta_2 = \Delta\beta = \frac{2\pi}{\Lambda}, \quad (3)$$

where Λ is the periodicity of the grating, β_1 and β_2 are the propagation constants of coupled modes, and $\Delta\beta$ is the difference in the propagation constants of the coupled modes.

When the period of the grating is chosen in a way to facilitate coupling between forward propagating mode ($\beta_1 = \beta$) and its reverse direction propagation counterpart ($\beta_2 = -\beta$), the condition (1) can be described as $\beta = \pi/\Lambda$, which can also be rewritten as $\lambda = 2n_{\text{eff}}\Lambda$, where n_{eff} represents the effective index of the mode, and λ is the wavelength, in which coupling occurs. This approach is usually referred to as “conventional” FBG. Wavelength λ in which coupling occurs depends on the period Λ and n_{eff} . Conventional FBGs are, therefore, sensitive to mechanical strain (length changes cause period Λ to change) and temperature (n_{eff} depends directly on the core RI change), but not to other (external) parameters.

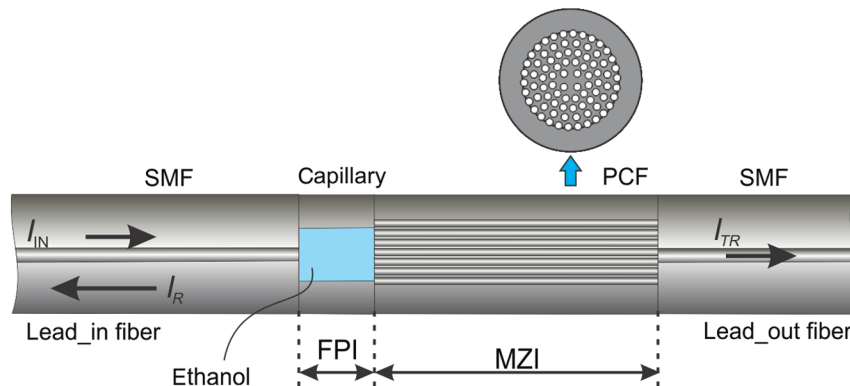


Fig. 19 All-silica RI-temperature sensor.

To satisfy coupling conditions in “standard” FBGs, the period Λ of conventional FBGs needs to be short, comparable to operating wavelength, i.e., $\Lambda = \lambda/2n_{\text{eff}}$. On the other hand, the period of the grating can be made much longer (e.g., in the mm range). This will facilitate coupling among the modes that have very similar phase constant β . These LPFBGs can be used to couple modes efficiently within a few mode or multimode fibers, or to couple guided modes with the cladding modes of the fiber that all propagate in the same direction. For sensing applications, it is of particular interest to facilitate coupling among fundamental modes of the single-mode fiber and cladding mode(s) of the same fiber. Cladding modes extend their (evanescent) fields beyond the fiber’s outer edge and are sensitive to variation of the RI in the fiber’s surroundings. In the latter case, the fiber’s surrounding RI variation modulates phase constants of the cladding modes, which leads to shifts in the wavelength characteristics of the LPFBG. The coupling condition for an LPFBG can also be described as

$$\frac{2\pi}{\Lambda} = \frac{2\pi}{\lambda} (n_{\text{eco}} - n_{\text{ecla}}^i), \quad (4)$$

where n_{eco} is the effective index of the fundamental core mode (or any other mode that guides light into the sensor structure), n_{ecla}^i is the effective index of the i ’th cladding (or higher-order guided) mode, λ is the resonance wavelength, and Λ is the period of the grating.

The third type of FBGs encountered in multiparameter sensors is tilted FBGs. Here an FBG with a short period is inscribed into fiber’s core at a slanted angle. Tilted FBGs are usually employed to couple a forward propagating mode efficiently with one or multiple back-propagating cladding modes; however, if the tilt angle exceeds 45 deg, coupling is also possible with the forward cladding modes.

It is straightforward to use FBGs, LPFBG, tilted FBGs, and their combinations^{47–51} to sense different sets of parameters. Furthermore, all types of FBG/LPFBG and tilted FBG sensors can be interrogated very straightforwardly by spectrally resolved interrogators. In these cases, individual FBGs, which constitute multiparameter sensors, possess different characteristics’ wavelengths and are usually made preferentially sensitive to individual sensed parameters. Preferential sensitivity, however, usually implies that different sensors’ gratings possess different sensitivities to parameters being sensed simultaneously, rather than exhibiting highly selective sensitivity to each of the sensed parameters. This is because the influence of certain parameters, for instance temperature, cannot be eliminated from grating sensitivity. For example, a grating-based sensor for simultaneous RI and temperature measurements usually employ one grating that is sensitive to temperature and one grating that is sensitive to both RI and temperature (it is exceptionally difficult to design a compact and temperature-independent grating, especially if it needs to be sensitive to RI). Thus the matrix method or similar post-processing of spectral data is needed in most cases to resolve sensed parameters independently of each other.

2.4.1 Types and designs of grating-based multiparameter sensors

Common FBG multiparameter sensors are designed to measure temperature and strain simultaneously.^{52–60} One of

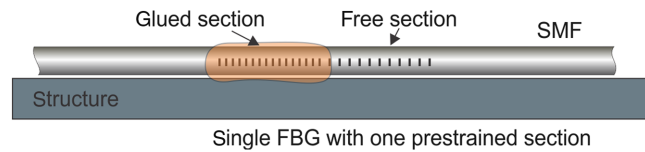


Fig. 20 Strain and temperature sensor with single FBG.

the earliest dual-parameter FBG sensors was based on a single FBG. Part of the FBG was preloaded and glued to the surface (strain measuring part), while part of the FBG was unattached/free and provided a temperature measuring part,^{56,57} as shown in Fig. 20.

In many cases, the strain is related to other parameters, like force, bending radius, torsion, and similar mechanical quantities. In these cases, strain is usually measured at multiple points/locations on the measurement object or body, while the changes in strain at these points are different, or even have the opposite in sign. In these cases, the temperature and strain-related parameter can be obtained by adding and/or subtracting shifts in the characteristic wavelengths of individual FBGs, similarly as is done with conventional resistive strain gauges. An example of bending/load measurement using this approach is shown in Ref. 58, where gratings experience compressive and tensile strains under load/bending, resulting in equal but oppositely signed wavelength shifts, which are used for temperature (by adding both wavelength shifts) and strain/bending (by subtracting both wavelength shifts) determination, as illustrated in Fig. 21.

Strain and temperature can also be measured simultaneously using two uniform FBGs with different cladding diameters,^{55,60} as shown in Fig. 22. In this case, the FBGs exhibit the same temperature sensitivities, but different responses to strains. Use of this approach requires fixation of sensors in two localized regions, i.e., on each side of the sensors (i.e., “spots welding”). The difference in fiber diameters causes different strain build up along both fibers/gratings, which makes a difference in FBG characteristics wavelength responses.

An alternative similar and interesting approach is to splice together two fibers with dissimilar temperature sensitivities (i.e., fibers with different thermo-optic coefficients), and then inscribe an FBG over the splice region.^{53,54} This leads to the formation of two FBG sections having different temperature sensitivities, while the strain responses for both fibers/gratings sections remains unaltered, which provides possibilities for unambiguous strain and temperature resolution. Different temperature sensitivities of individual fibers were achieved in reported works, either using two fibers with different germanium doping levels,⁵⁴ or by combining standard germane-silicate fiber with boron-co-doped fibers (boron doping increases the coefficient of thermal expansion of silica glass, which results in string temperature-dependent stress build up in the core, which leads to high-temperature sensitivity).⁵³

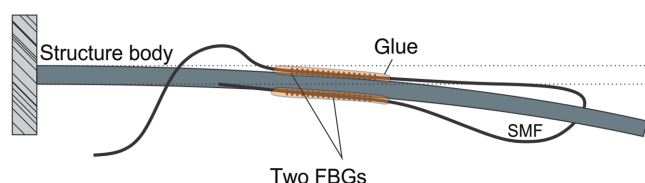


Fig. 21 Bending and temperature sensor using two FBGs.

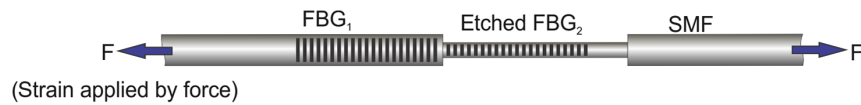


Fig. 22 Strain and temperature sensor based on two FBGs with different outer diameters.

Another possible use of FBGs includes chirped FBGs. Liu et al.⁶¹ described a system where a chirped FBG is inscribed in a section of HB fiber. When both polarization modes are excited in such chirped FBG inscribed HB fiber section, they interfere along the fiber/grating, which causes sinusoidal modulation of the back-reflected optical spectrum. When this fiber section is exposed to a strain, the sinusoidal modulation will maintain the period, but will shift in a spectral domain as the phases among both polarization modes and the period of the grating are changed. On the other hand, chirped FBG also responds to both strain and temperature (i.e., an envelope of spectrum in the back-reflected signal, which defined by the FBG characteristics period, is shifting with temperature). Proper signal processing of a back-reflected optical spectrum allows for determination of strain and temperature.

Another approach is to use two superimposed FBGs having two substantially different characteristics' wavelengths.⁵⁹ Each of the two superimposed gratings are subject to the same temperature and strain variations, but due to the wavelength dependency of the photoelastic and thermo-optic coefficients, wavelength changes of the two gratings were different. Different strain sensitivities of two FBGs were also achieved by prestressing the photosensitive fiber, in which the FBG is inscribed.⁵²

A further larger group of multiparameter sensors based on FBGs are sensors for simultaneous measurements of pressure and temperature.⁶²⁻⁶⁷ The approach described in Ref. 62 utilizes a design with partially polymer-coated FBG, which increases the pressure and temperature sensitivities significantly. Another similar example, depicted in Ref. 63, presents a pair of gratings coated with different polymers (Fig. 23), one polymer to enhance pressure, and the other to enhance temperature sensitivity.

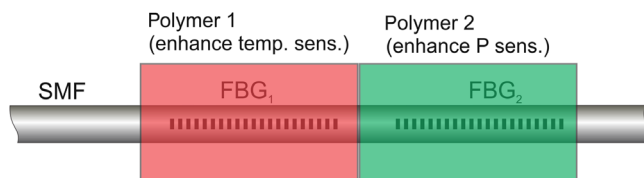


Fig. 23 Pressure and temperature sensor based on two FBGs-coated with different polymers.

In Ref. 65, a combined FBG and LPFBG are embedded into an elastic polymer material, which is deformed under pressure and, consequently, strains both gratings. The difference in sensitivities of both gratings is used to resolve pressure and temperature. The approach described in Ref. 64 contains a glass cantilever structure that further contains two FBGs that can be used for bending and temperature determination, as described in Ref. 58. An additional approach to increase pressure-sensitivity of fiber FBGs is to inscribe them in proper microstructure fibers, which exhibit higher pressure sensitivities. Stacking of a microstructure fiber with SMF while inscribing FBGs in both fibers leads to dual-parameter sensors. An example of this approach is described in Ref. 66, where one grating is written in a standard SMF, and the other into a pressure-sensitive microstructured "grapefruit" fiber. A similar approach, based on specialty pressure sensitized fibers, is presented in Ref. 67. In this case, two FBGs are inscribed in a specialty hollow fiber that contains two different cladded cores with different sizes; thus the pressure and temperature coefficients of both FBGs are different.

A few multiparameter sensors based on FBGs capable of measuring displacement and temperature were presented.⁶⁸⁻⁷⁰ A simple example employs an FBG mounted on a specially designed cantilever beam (Fig. 24), which consists of two sections having different, but uniform, thicknesses.⁶⁸ An FBG is mounted onto the beam along its axis in a way to cover both beam sections, which results in two FBG sections with different strains, but equal temperature sensitivities and enables measurement of displacement and temperature simultaneously.

A further similar example, based on an FBG sensor mounted on a bilateral cantilever beam, is described in Ref. 69, where the two parts of the beam are influenced by opposite strains (displacement) leading to a red shift for the part of the FBG subjected to compression, and to a blue shift for the part leading to elongation. A similar approach is described in Ref. 70, where an FBG is glued onto the inner surface of a thin-walled ring. When the ring is deformed (part of the ring is compressed and part elongated), it splits the FBG into two segments with two identical, but opposite, directed chirp gradients, which induces distinctive spectral modulation within the broadened spectral peak. Proper processing of the spectrum can be then used to resolve temperature and displacement independently.

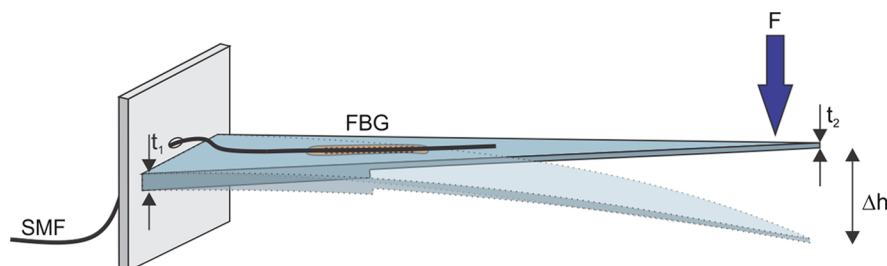


Fig. 24 Displacement and temperature sensor based on an FBG mounted on a cantilever beam.

FBGs are also used to build multiparameter sensors for simultaneous measuring of RI and temperature.^{71–74} FBGs are usually made sensitive to RI by exposing the fiber core with an inscribed FBG to a measured medium. Thus these sensors differ mainly in the method that is used to provide the core-exposed FBG region. A straightforward approach, utilizing a side polished fiber section, is described in Ref. 71. Here two FBGs are utilized; one FBG is written into the side-polished SMF to allow sensing of the surrounding RI; another FBG is written in the nonpolished SMF section to serve as a temperature sensor. Another similar approach is reported in Ref. 72, where a fiber section containing FBG was wet-etched in order to expose the core. Wet etching is also used in Ref. 74, where a short section of fiber/FBG (shorter than the initial FBG length) is etched down to the core size. This creates two peaks in the reflection spectrum of the FBG. Since both peaks exhibit different temperatures and RI sensitivities, temperature and RI can be measured simultaneously. A further similar approach⁷³ includes side polishing, but in this configuration, the entire grating section is polished, and then only half of its length is overlaid by the measured liquid material (Fig. 25), which results in dual peaks in the Bragg spectrum, which allow for RI and temperature measurements.

Measurement of force and temperature is another area where FBGs offer straightforward solutions. In Ref. 75, an FBG is affixed on the nonuniform strain area of a double-hole cantilever beam, which resulted in wavelength and spectral peak width dependency on the applied force, while temperature changes just led to a shift in the reflected wavelength.

A method for simultaneous measurement of bending and temperature is presented in Ref. 76, using a sampled chirped FBG (LPFBG with multiple segments having different periods) with multiple resonant peaks. In this case, the FBG is fixed onto a flexible cantilever beam. When the temperature along the chirped FBG is increased, multiple resonant peaks of the grating shift uniformly toward longer wavelengths, since the chirp ratio along the sampled chirped FBG is not changed by the temperature change. Exposure to bending, however, compresses or expands peaks' positions in the spectrum. This allows discrimination of both measured parameters.

In addition to conventional FBGs, LPFBGs, and also tilted FBGs, are also encountered frequently in multiparameter sensors. LPFBGs and tilted FBGs add versatility to the grating approach, because they allow for local interaction with cladding modes, which can provide a broader range of possibilities for interaction with the sensor's surrounding. LPFBG and tilted FBG sensors are encountered for simultaneous measurements of temperature and RI,^{77–83} temperature and strain,⁸⁴ temperature and bending curvature,⁸⁵ and

as sensors for rotation and displacement⁸⁶ measurements. LPFBGs also allow for design of sensors that combine measurements of parameters that are otherwise difficult to measure by fiber-optic approaches, e.g., sensors for simultaneous measurements of liquid level and temperature.⁸⁷

The most frequently reported combination of parameters sensed by multiparameter LPFBG sensors are RI and temperature sensor. There are several approaches to distinguish those two parameters. Perhaps the most straightforward way is described in Ref. 80, where a pair of LPFBGs with different periods is inscribed side-by-side in a single piece of dual-cladding fiber. LPFBG periods were chosen in a way that one of LPFBGs couples core mode with inner cladding modes, while the other couples the core mode with the modes of the outer cladding. This assures that one of the LPFBGs is sensitive to temperature only, while the other is sensitive to temperature and RI. A similar approach is presented in Ref. 78, where two LPFBGs having different grating periods were inscribed in SMF instead. The fiber region containing the second LPFBG is chemically etched to act as a highly sensitive RI sensor [Fig. 26(a)], whereas the first LPFBG possesses similar temperature sensitivity as first one and can act as a reference. A similar approach⁷⁷ is realized by two LPFBGs inscribed in different fibers, one in SMF and the second in double-clad fiber, as shown in Fig. 26(b). The LPFBG section in the double-cladding fiber is solely sensitive to temperature, while the section of the LPFBG in the SMF is sensitive to both temperature and surrounding RI. Another approach⁷⁹ is based on a single-ultralong LPFBG, which possesses multiple resonance peaks. These peaks possess different temperatures and RI sensitivities.

Further examples, Refs. 81–83, present RI–temperature sensors based on tilted FBGs (Fig. 27), which, in comparison to standard FBGs, provide relatively high sensitivity to RI without any additional need for intervention to the fiber geometry, in which they are inscribed. Tilted FBGs usually form a complex back-reflected optical spectrum, which is composed of many peaks. For example, in a standard single-mode fiber and for grating tilts of <45 deg, these peaks correspond to resonance coupling among forward propagating fundamental mode, and a variety of backward propagating modes that usually include both backward propagating fundamental mode and variety of cladding modes. In this case, resonance coupling between the forward and backward propagating fundamental modes is temperature-dependent, but independent of RI, whereas resonances among the forward propagating mode and variety of backward propagating cladding modes exhibit strong dependence on surrounding RI and temperature. Cladding modes responses are further dependent on the mode order and grating properties. Thus proper signal processing of a part of

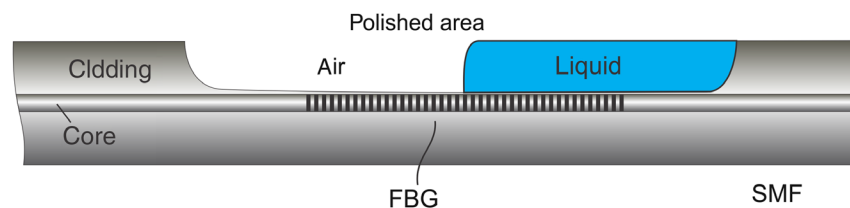


Fig. 25 RI and temperature sensor based on polished FBG partially covered by liquid.

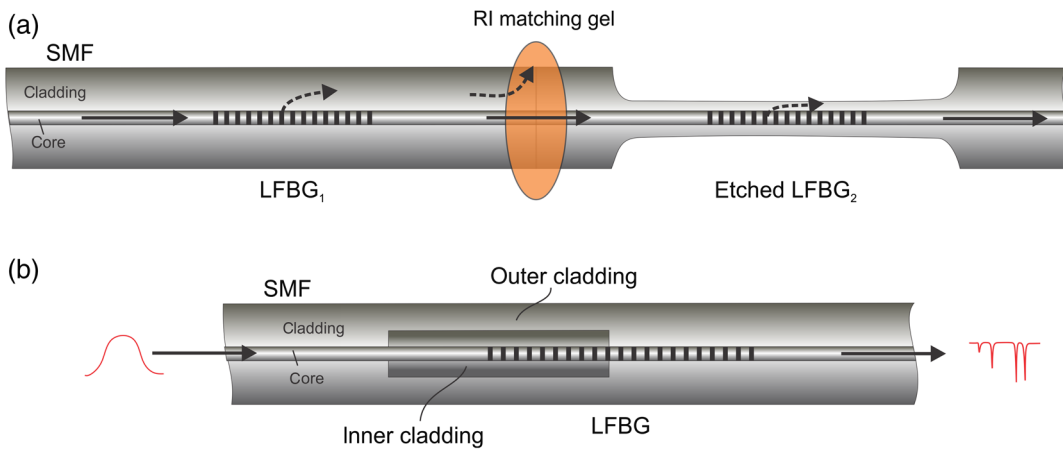


Fig. 26 RI and temperature sensors based on LPFBGs: (a) LPFBGs having different periods and (b) LPFBGs inscribed in dual-cladding fiber.

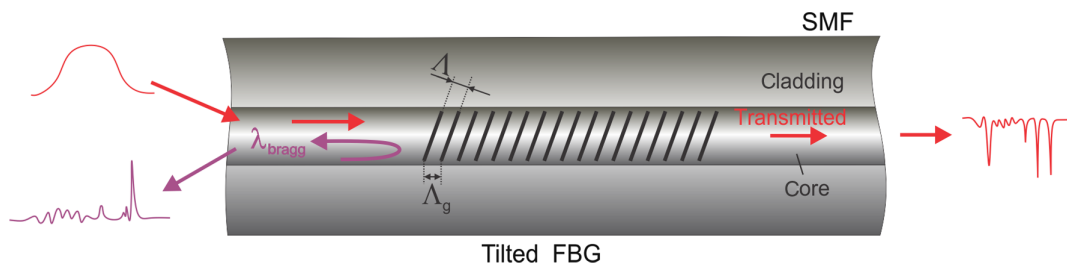


Fig. 27 Typical example of tilted FBG used for multiparameter sensing.

the entire back-reflected spectrum is used to extract temperature and RI independently of each other. Examples of this approach are presented in Ref. 82.

Tilted multimode FBG can also be used to design dual-parameter RI–temperature sensors as described in Ref. 81. In this case, two different groups of resonances appear in the transmission spectra, one that belongs to coupling among forward and backward propagating core modes, and the other belonging to coupling among core and cladding modes. These transmission dips caused by mode coupling between core and cladding modes are sensitive to surrounding RI and temperature, whereas the dips due to the coupling among core modes are sensitive only to temperature. Proper signal processing of the spectrum is again needed to resolve information on RI and temperature unambiguously. Another sensor design utilizes FBG and tilted FBG inscribed one over another to form a tilted moire FBG,⁸³ as illustrated in Fig. 28. Using a single-tilted moire FBG sensor, the temperature change can be obtained directly from the wavelength shift of the back-coupled fundamental mode (Bragg mode), whereas the RI modulates resonance wavelengths

belonging to the coupling between the fundamental and cladding modes.

Sensors for measuring temperature and strain simultaneously⁸⁴ present another group that can be realized by tilted FBGs or LPFBGs. An example of a single-tilted LPFBG use for simultaneous strain and temperature sensing is described in Ref. 84. The core mode and cladding modes' resonances have equal temperature, but different strain sensitivities. Thus proper monitoring and comparison of the core-mode resonance with the cladding-mode resonances allows for unambiguous separation of temperature and strain. A simultaneous force and temperature sensor based on LPFBG was presented in Ref. 88. The LPFG was inscribed over the splice between a microstructured optical fiber and a standard SMF. The grating exhibits two groups of attenuation bands with different responses to temperature and strain. The presented sensor is relatively long, i.e., its length exceeds few centimeters.

Simultaneous sensing of temperature and bending/curvature was reported in Ref. 85. This approach utilizes observations of amplitude changes of different transmission dips

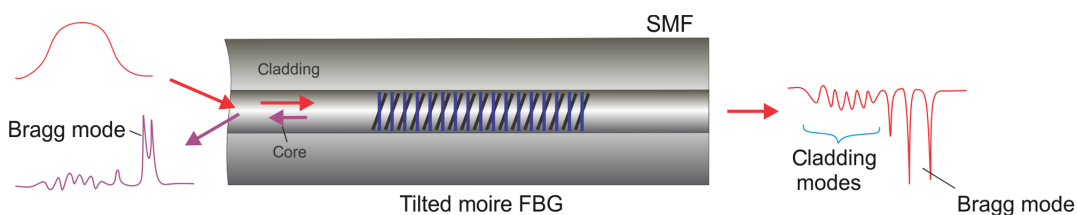


Fig. 28 RI and temperature sensor based on a single-tilted moire FBG sensor.

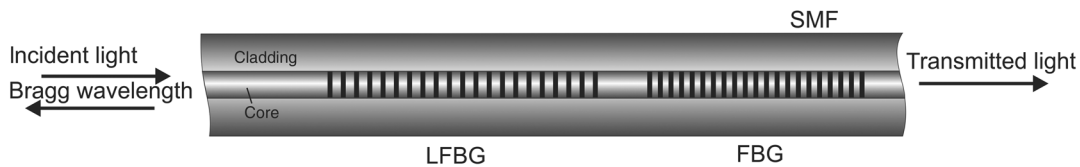


Fig. 29 RI and temperature sensor based on cascaded LPFBG and FBG.

related to two types of LPFBG, spliced together and inscribed into two different types of fibers (one inscribed into an H_2 loaded fiber, while the other inscribed in a B₂/Ge-doped fiber). In this case, increased fiber bending modulates cladding modes losses in both fibers, which further leads to modulation of resonance dips' amplitudes in both gratings. The temperature, on the other hand, also affects the amplitudes of the gratings' spectral dips, but distinctively for both types of gratings. To overcome the problems of crosstalk and nonlinearities in the proposed sensing system, an artificial neural network was trained to distinguish among both measured parameters.

A sensor for simultaneous rotation and displacement (bending) measurement based on a tilted FBG is described in Ref. 86. Cladding modes are sensitive to torsional fiber/twist due to the stress build up in the cladding that is induced by fiber rotational twisting. The magnitude of these effects is proportional to the distance from the center of the fiber thus the higher-order modes usually see stronger modulation of their effective indices during the fiber's torsional twist, which leads to modulation of peaks in the spectrum of the LPFBG. On the other hand, fiber bending alone modulates cladding modes' effective indices and LPFBG resonances. The method described in Ref. 86 observes selected cladding mode resonances, which exhibit different sensitivities to the curvature and rotation and are correlated further to the rotation and curvature of fiber bending. A very similar approach is presented in Ref. 89, where the interference among multiple modes of an elliptical hollow-core photonic bandgap fiber is utilized to obtain simultaneous fiber twist and temperature measurements.

Access to cladding modes through tilted FBGs also allows for a design of sensor for simultaneous measurement of liquid level and temperature.⁸⁷ In this case, both parameters can be measured avoiding undesired crosstalk by tracking the difference in responses of core and cladding modes' resonances. In particular, temperature variations are related to the core mode resonance wavelength, while the variation in the liquid level is correlated to an integral of amplitudes of all cladding modes that are present in the sensor's transmission spectrum.

In many instances, combinations of conventional FBGs and LPFBGs prove to be a convenient approach in the design of multiparameter sensors. Sensors for simultaneous measurement of RI and temperature certainly belong to this group.^{48,49} The approach described in Ref. 49 utilizes an LPFBG and an FBG written one after another in a D-fiber. The FBG is sensitive to temperature, whereas the LPFBG, which provides cladding mode resonance, responds to both RI and temperature. Additional thinning of the D-fiber through the etching process further allows for sensitivity tuning and sensitivity enhancement. A similar approach is also reported in Ref. 48, where a cascade of LPFBG and FBG are formed near the tip of a single-mode fiber

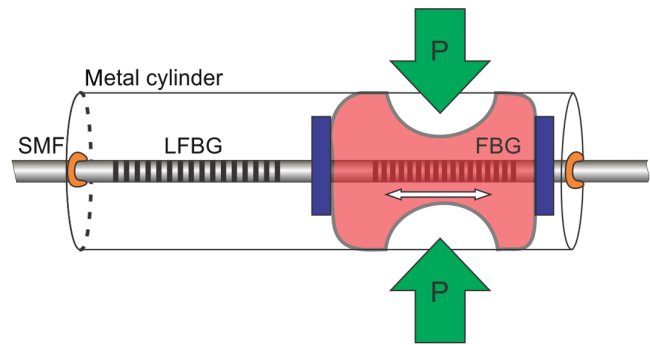


Fig. 30 Pressure and temperature sensor based on LPFBG and FBG encapsulated in a metal cylinder.

(Fig. 29). By simply measuring wavelength shifts in transmission dips of both gratings, one could establish temperature and RI. Interestingly, when the sensor is properly designed, and when observing the back-reflected spectrum which contains only the FBG wavelength, the amplitude of the spectral peak becomes proportional to RI, whereas the characteristics' wavelength depends only on the temperature, which might allow for a simple sensor interrogation scheme.

Combinations of LPFBG and FBG can also yield sensors for simultaneous temperature and pressure sensing. Wang et al.⁵¹ represented an example where a fiber with closely inscribed LPFBG and FBG is encapsulated in a metal cylinder with two side openings, each on opposite sides of the cylinder wall (Fig. 30). The external pressure compresses the polymer region around the opening, which causes mechanical deformation of the polymer and change in its RI. In this case, both gratings respond differently to mechanical deformation, surrounding RI change, and temperature. Observation of both grating characteristics' wavelength consequently allows for independent determination of pressure and temperature.

A combined FBG-LPFBG sensor was also reported for simultaneous measurement of relative humidity and RI.⁴⁷ The sensor consists of two gratings stacked in series, from which the LPFBG is polyimide coated to enhance relative humidity sensitivity, while the conventional FBG is used for measurement of temperature.

2.5 Multiparameter Sensors Based on Combinations of FBG/LPFBGs and FPIs

FBGs combined with FPIs usually to provide opportunities for measurements of parameters that involve combinations of pressure and temperature,^{90,91} strain and temperature,⁹²⁻⁹⁵ and RI and temperature.⁹⁶⁻¹⁰⁰ FP cavities are especially convenient for the design of pressure-sensitive sensor sections and are often realized in different configurations.

Simple cascading of an FPI and a conventional FBG can provide a straightforward way to create a dual-parameter

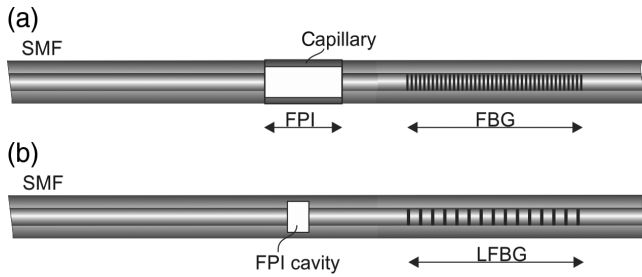


Fig. 31 Strain and temperature sensors based on: (a) cascading FPI and FBG and (b) cascading FPI and LPFBG.

sensor. For example, in Ref. 93, an in-line fiber etalon (created by silica capillary splicing in-between two SMFs) is cascaded with an FBG to form strain/temperature sensors [Fig. 31(a)]. An in-line fiber etalon is strain sensitive, but has low-temperature sensitivity, while an FBG is sensitive to both temperature and strain. A matrix method is then used to resolve both parameters. A similar approach is also described in Ref. 94. An alternative approach is presented in Ref. 91, where pressure is determined through gas RI measurements, which are performed by a short-open-path cavity, while an FBG is added into a cascade with an FPI to provide temperature measurement and the compensation required for extraction of pressure from the gas RI variation. It is also possible to cascade FPI with LPFBGs⁹⁵ as shown in Fig. 31(b). Since an LPFBG can be inscribed in a way to allow high-temperature LPFBG operations, this approach might be advantageous in multiparameter sensors for high-temperature sensing applications.

A further approach in a design of combined FPI-FBG sensors is to use two closely spaced FBGs, which define a sensing FPI among both gratings as illustrated in Fig. 32(a). A structure like this provides a distinctive spectral response, which is composed of overlying the spectra of both the FBGs and FPI. Proper signal processing, which usually involves matrix method, can resolve characteristics' wavelengths of

FBGs and path length variation in the FPI defined by the FBG pair. A combined strain–temperature sensor can be realized in this way, as described in Ref. 92. A similar approach can also be used to build a sensor for pressure and temperature sensing.⁹⁰ In this case, a short section of PCF fiber is inserted in-between two SMFs containing FBGs to create a pressure-sensitive FPI [Fig. 32(b)]. The surrounding pressure compresses the PCF region and produces a distinctive spectral response, while the shift in FBGs' wavelength is used mainly to determine the temperature.

Another straightforward approach was presented in Ref. 101, where an temperature-sensing FBG and diaphragm-based-pressure-sensitive FPI are stacked on the tip of an SMF. Pressure-sensitive FPI is made out of a short-glass capillary and a silica diaphragm. Pressure is measured by a combination of a laser diode and a photodetector, using quadrature point measuring scheme, while the temperature information is obtained by back-reflected spectrum analysis of FBG peak position.

In a similar way, simultaneous RI and temperature sensing was described in Ref. 97, by creating a micromachined, open-path cavity in-between two identical FBGs. Another interesting example of a structure utilizing closely spaced FBGs, which define a sensing FPI, is obtained when the fiber between both gratings is tapered in a way to allow for evanescent field interaction within the tapered region, as described in Ref. 98. This allows for the creation of combined RI–temperature sensors with low insertion losses. Low insertion loss allows multiplexing of multiple sensors located along a single fiber.⁹⁹

A rather special example of a sensor based on a combination of FPI/FBG is presented in Ref. 96, where a single FBG is used to define dual FPIs within the same birefringent fiber (individual interferometers are defined by linear polarization modes of birefringent fiber). Proper processing of spectral response allows, in this case, simultaneous sensing of temperature and RI.

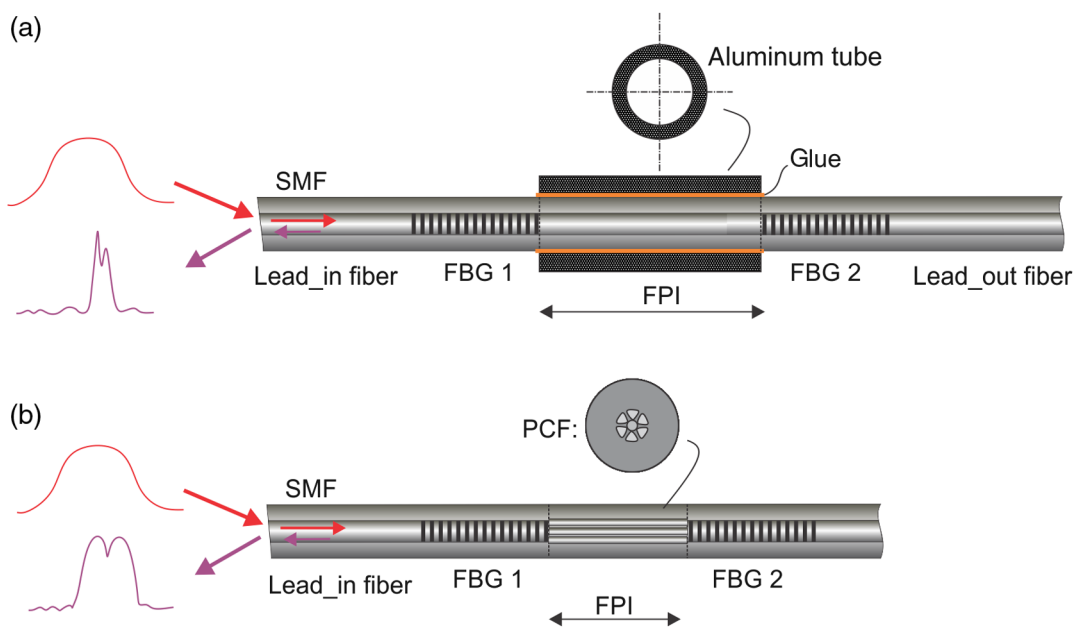


Fig. 32 Pressure and temperature sensors based on: (a) FPI cavity from SMF sandwiched between two FBGs and (b) FPI cavity from the PCF sandwiched between two FBGs.

2.6 Multiparameter Sensors Based on Combinations of FBGs and MZIs/Michelson Interferometers

Combinations of FBGs and MZI (or MI), predominantly, provide opportunities for building of sensors for simultaneous sensing of temperature and RI. While there is a substantial number of different reported variations of RI-temperature sensors that utilize MZI and FBG/LPFBG combinations,^{102–117} mostly they share the same operational principle: MZIs are created by one of the methods described in Sec. 2.2 and are sensitive to both external RI variation and temperature, while FBGs are predominantly used as temperature sensing sections (in case of LPFBG, spectral features corresponding to LPFBG resonance also become RI-dependent, but this dependence is considerably lower than the spectral sensitivity of the modal interference caused by modes that are coupled by LPFBG into the cladding). A rather special case of this approach is described in Ref. 118, where the fiber section containing FBG is bent strongly (Fig. 33). Strong bending couples light into the cladding, and this light interferes with the mode propagating within the core, which provides the desired RI sensitivity.

Proper design of these sensors can also keep overall insertion losses at a sufficiently low level to allow multiplexing of this type of sensor reported in Ref. 110.

A similar design with strongly bent fiber is presented in Ref. 119, where the sensor is created out of a strongly bend (balloon-shaped) single-mode fiber, which forms a displacement-sensitive MZI (in the bend, light is coupled from core to cladding modes that further interfere with a core mode) and an LPFBG. The sensor has two distinctive spectral dips, which respond to displacement and temperature with different sensitivities and allow for discrimination of both parameters.

Another alternate design of MZI-LPFBG type of RI-temperature sensor is presented in Ref. 120. Here a liquid-filled PCF, which forms an MZI, is cascaded with an LPFBG. The

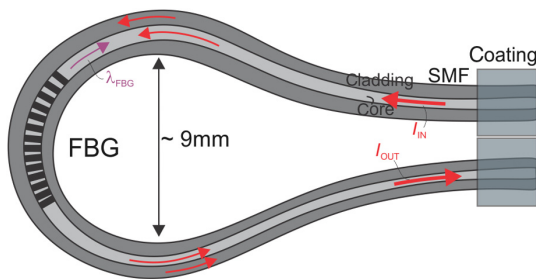


Fig. 33 RI and temperature sensor based on a strongly bent FBG.

liquid-filled PCF is only sensitive to temperature change, while the resonant wavelength shift of the LPFG responds to both RI and temperature.

LPFBGs and MZIs can also be combined to form sensors for simultaneous strain and temperature sensing, as described in Ref. 121. This design involves a double-cladding fiber with two LPFBGs inscribed apart, so that strain is applied only between both LPFBGs (Fig. 34). The transmission spectrum is composed of LPFBG resonance dips that are further modulated by MZI interference fringes, i.e., grating resonances present an envelope for MZI interference fringes. In this configuration, a change in ambient temperature causes a shift in the position of the LPFBG spectral dips (spectral envelope), while the strain application causes a change of phase of the MZI fringes, which are observable (enveloped) within the FBGs dips. Tracing of a spectral envelope allows for temperature determination, whereas tracing of fringes within the LPFBG envelope allows for correlation with strain.

A further approach to measure strain and temperature is described in Ref. 122, where a sensor is based on a standard FBG, and an intermodal interferometer based on a PCF. The intermodal interferometer exhibits an opposite strain response compared to that of the FBG. It also exhibits high sensitivity to strain, while it is relatively insensitive to temperature. These characteristics are used for the discrimination of strain and temperature signals, and for improving strain and temperature measurement resolutions.

Combinations of FBGs and MZIs also allow for the design of three-parameter sensors that can measure strain, RI, and temperature, simultaneously. In Ref. 123, an FBG is inscribed into a dual-mode fiber. An FBG like this not only possesses two characteristic Bragg resonances, which exhibit different sensitivities to strain and temperature and correspond to backward coupling of LP01 and LP11 modes, but also shows many strong cladding mode resonances, which are all sensitive to RI. Another similar example of a three-parameter sensor (strain, RI, and temperature) is reported in Ref. 124, where the sensing structure is composed of three regions (Fig. 35): (a) a single-mode fiber with inscribed FBG, which is only strain and temperature sensitive, (b) a tapered SMF section with inscribed FBG, which is sensitive to temperature, strain, and RI, and (c) a section of coreless fiber (that defines MZI), which is also sensitive to all three-sensed parameters, but with considerably different spectral sensitivities to all three parameters than the FBG inscribed in the tapered region. Proper processing of the transmission/refraction spectrum using the matrix method then leads to a measurement system that can distinguish all three parameters.

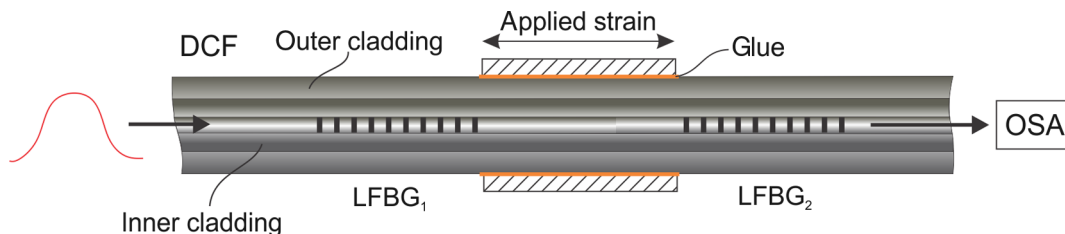


Fig. 34 Strain and temperature sensor based on an LPFBG inscribed in a double-cladding fiber.

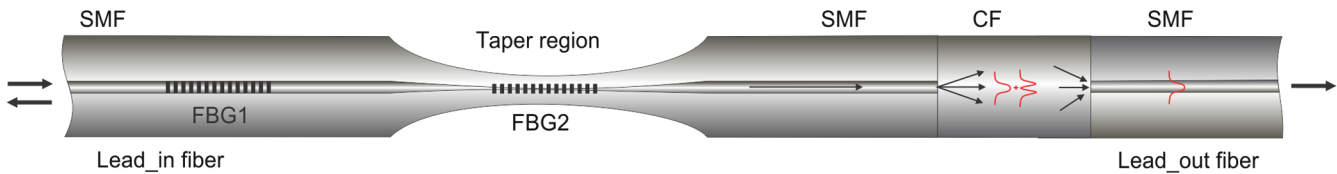


Fig. 35 Strain, RI, and temperature sensor.

2.7 Multiparameter Sensors Based on Fiber Loops

A fiber loop mirror is a fiber structure that can support several sensor configurations for multiparameter sensing. Fiber loops include a 3-dB directional coupler and a section of HB fiber that generates an optical path-length length difference within the loop and allows interferometric sensing of changes in the HB fiber’s birefringence.

Fiber loops can serve as combined sensors for strain and temperature measurements. The approach reported in Ref. 125 describes a sensor that consists of two consecutive, but different, sections of HB, configured into a fiber loop mirror, which creates multiple interference paths with the loop that exhibit different sensitivities to strain and temperature (strain and temperature are then resolved by proper processing of the Interferometer’s spectral response). Another fiber loop-based approach is described in Ref. 126, and utilizes a method where a high-power pump laser is inserted into the fiber loop to change the properties of the HB erbium-doped fiber (Fig. 36). With the different sensitivity responses of the erbium-doped fiber to strain and temperature when the high-power pump laser is ON or OFF, it is possible to measure these two physical parameters simultaneously.

A polarization maintaining PCF configured into a loop mirror that acts as a strain sensor together with an erbium-doped fiber¹²⁷ that acts as a temperature-dependent amplified spontaneous emission (ASE) source also allows for combined strain and temperature sensing. Here, measuring the

spectral position of the loop interference peak responds to temperature and strain, while the power/amplitude of the same peak correlates to temperature only. Further loop configuration for simultaneous strain and temperature measurement is reported in Ref. 128. The sensing head is composed of a fiber loop mirror incorporating a section of FBG, which is inscribed into the polarization maintaining fiber and signal loop interference fringe (generated by the inserted polarization maintaining fiber) show different sensitivities to strain and temperature, which allows for discrimination of strain and temperature using the matrix method.

Another sensor example, described in Ref. 129, is apt to measure temperature and humidity simultaneously. It uses a fiber loop that contains a short section of HB fiber with inscribed LPFBG as shown in Fig. 37. The surface of the fiber with the LPFBG is coated with moisture-sensitive polyvinyl alcohol, which changes RI proportionally to relative humidity. The resonance wavelength and its intensity vary with temperature and humidity, so humidity and temperature can be measured simultaneously.

The next example presents a combination of PCF and fiber loop mirror to form a hydrogen/RI and temperature sensor.¹³⁰ Hydrogen sensitivity was archived by Pd/WO3 coating of PCF, which formed amodal interferometer, while the loop configuration of, otherwise, HB PCF provided temperature sensitivity.

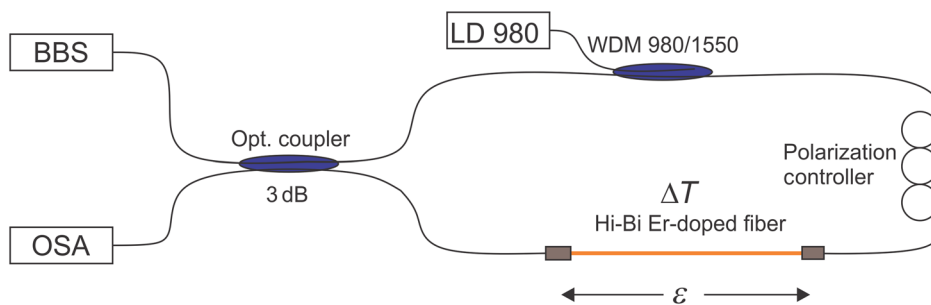


Fig. 36 Strain and temperature sensor based on HB erbium-doped fiber.

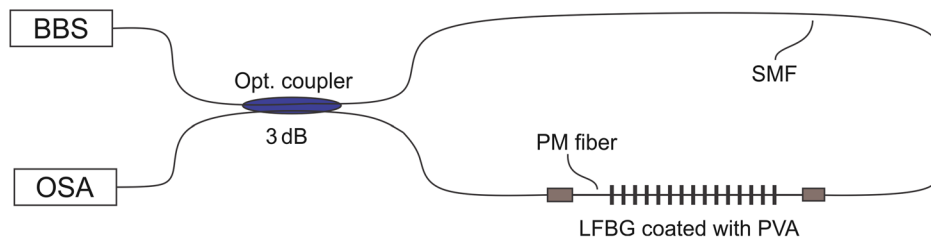


Fig. 37 Humidity and temperature sensor.

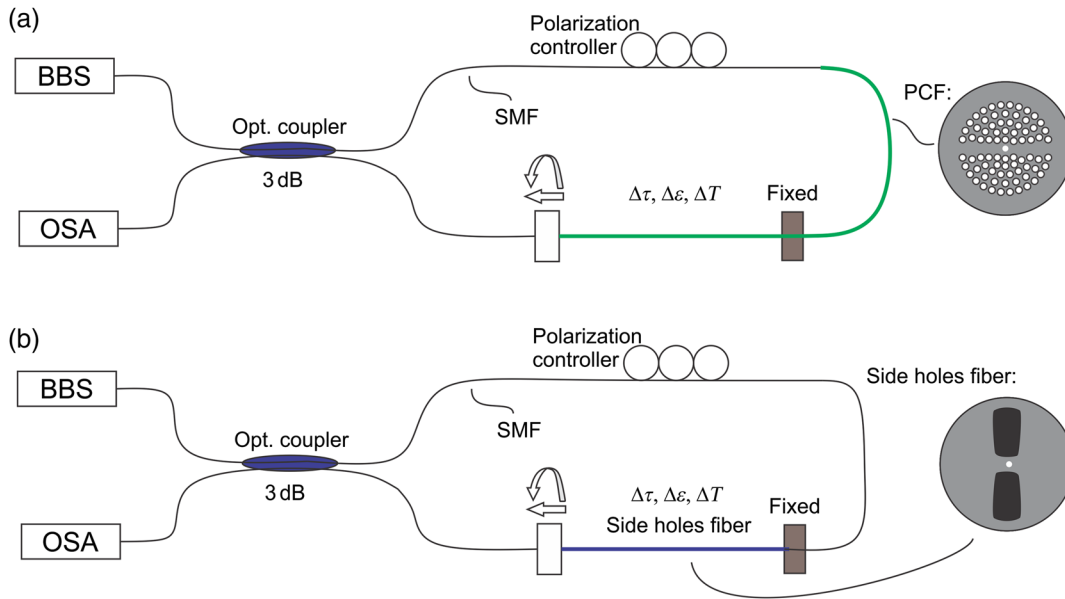


Fig. 38 Torsion, strain, and temperature sensor: (a) loop combined with an elliptical core PCF and (b) loop combined with elliptical core side hole fiber.

Fiber loops (Fig. 38), when combined with an elliptical core PCF¹³¹ or elliptical core side hole fiber,¹³² can also yield a sensor for simultaneous measurement of three parameters: the fiber’s torsional twist, temperature, and strain. In these reports, the elliptical core PCF or elliptical core side hole fiber exhibit group birefringence that is dependent on all three parameters. Due to the chromatic dispersion characteristics of the group birefringence in these fibers, the sensor possesses different wavelength responses to different parameters at different interference fringe valleys. The matrix method is then used to resolve all three parameters.

2.8 Multiparameter Sensors Based on Combinations of Interferometers and Intensity Modulation Principles

In certain instances, measurement of a sensor’s total reflectivity or reflectivity from a particular sensor’s surface can be used to determine an additional sensing parameter, mostly RI. This approach can be combined with most interferometric and grating principles that are otherwise utilized for measurement of other parameters (temperature, pressure, etc.).^{1,133–148} In more advanced designs, measurement of the reflection ratio from two adjacent sensors’ surfaces is utilized to reduce the sensitivity of the measurement to variability in interrogator-to-sensor interconnection losses and source variability. This is achieved through proper signal

processing that utilizes IDFT of back-reflected spectrum to determine and compare reflectance from multiple sensors’ surfaces,^{134,135,139} as shown in Fig. 39.

Sometimes, amplitudes of individual spectral features (peaks/dips), or interference fringe contrast, are correlated directly to the parameter that is measured, since the peak/dip amplitude and/or fringe contrast can often be associated with a particular surface’s reflectivity.¹⁴⁶ Examples of sensors where fiber interferometers or FBG are combined with reflectance monitoring from a particular surface to obtain simultaneous temperature and RI measurements are described in Refs. 1, 134–138, 140, 141, 144–146, and 148. A rather special case of an FBG-intensity modulation RI–temperature sensor is presented in Ref. 133, where a distributed Bragg reflector fiber laser is defined by two conventional FBGs, while the third tilted FBG is written in-between the cavity forming FBGs, as illustrated in Fig. 40. The tilted FBG acts as an intracavity loss modulator that depends on the surrounding RI, which affects the lasing properties of the laser.

An intensity-based approach combined with FBGs, using doped fibers, is also reported in Ref. 149, where an FBG is written into an Er:Yb:co-doped fiber. The fiber is pumped by a 980-nm source while observing the spectrum at the sensor’s output, and where the doped fiber acts as ASE source. Since ASE is temperature-dependent, the peak in the output

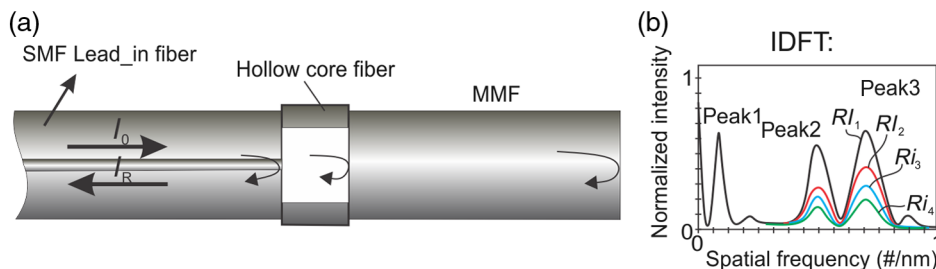


Fig. 39 (a) RI and temperature sensor and (b) its corresponding IDFT.

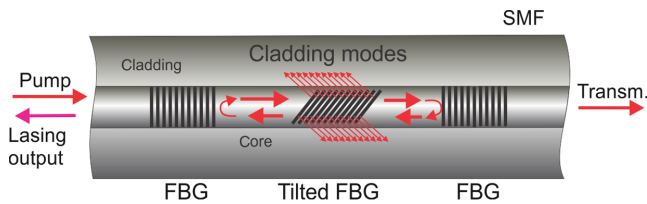


Fig. 40 RI and temperature sensor based on tilted FBG.

spectrum and the total output power can be correlated to the strain and temperature using the matrix method. Another example of combined interferometric and intensity-based measurement principle for simultaneous temperature and RI sensing is reported in Ref. 150. Here, an MI is formed using a conventional fiber directional coupler, but with one arm containing a short section of HB fiber as shown in Fig. 41. Spectral response contains, in this configuration, two distinctive features: a high-frequency finger corresponding to the optical path length difference among directional coupler arms, and a low-frequency fringe (which defines an envelope of high-frequency fringe) that corresponds to the interference among both polarization modes of the HB fiber. The position of the latter within the optical spectrum is predominately temperature-dependent, while the fringe contrast of the high-frequency fringe is RI dependent on the amount of back-reflected light from the exposed fiber end, which changes with RI.

More complex sensors for simultaneous measurement of three parameters (pressure, temperature, and RI) are reported in Refs. 139 and 143. The RI sensing function here is achieved through end-surface reflectance observation, as already described.

Another sensor for simultaneous measurement of three parameters (strain, temperature, and RI) is presented in Ref. 151. The sensor is based on a tilted FBG, where strain

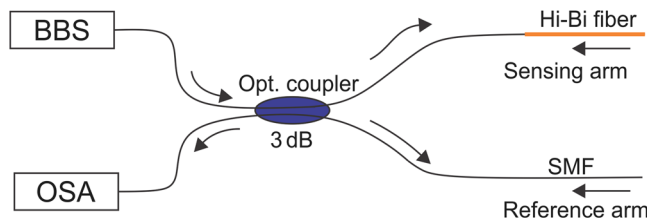


Fig. 41 RI and temperature sensor based on MI.

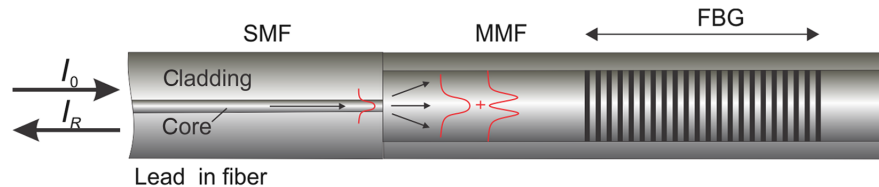


Fig. 42 Strain and bending sensor.



Fig. 43 A pair of HLPG.

and temperature are discriminated by observing the core mode and strongly guided cladding mode resonances, while the RI is determined by integration of the transmission spectrum.

Parameters other than RI can also be added to a set of parameters already measured by interferometric or FBG principles using intensity measurement approaches. An example of a sensor created along these lines is presented in Ref. 147, where a fiber loop is cascaded with an FBG. Modulation of the loop diameter (caused by linear displacement of the loop) and FBG spectral temperature response yields a sensor that can measure displacement and temperature simultaneously. A somewhat similar example of a sensor for simultaneous measurement of strain and bending is presented in Ref. 142. Here an FBG is inscribed in a short section of multimode fiber, while the fiber is excited by a single-mode fiber (Fig. 42). This causes the appearance of multiple peaks in a back-reflected spectrum, each corresponding to the FBG resonance of an individual mode. All these peaks are strain sensitive, but when the fiber is bent, their amplitudes change, due to the modal interference (it would be perhaps more correct to list this reference under Sec. 2f; however, the authors rely here on ratio-metric measurements, which make this sensor a combined intensity-FBG sensor).

Combining intensity modulation with FBG or interferometric principles might yield simple structures; however, these approaches still need spectral interrogation in most cases, while they suffer mostly from limitations that are typical for intensity based sensors. On the other hand, some reported RI-temperature sensors do not need any special post-proceedings (like matrix method) to discriminate between both measured parameters, which might certainly be an advantage in field applications. An interesting intensity modulation approach for measurements of fiber twist/rotation is presented in Ref. 152. Here a pair of helical long-period fiber gratings (HLPG) with opposite helicities was written into the sensing fiber (Fig. 43), resulting in two distinctive resonance peaks that exhibit oppositely signed spectral sensitivities to rotation and an equally signed response to the temperature. A pair of DFB diodes with different emission wavelengths, tuned to quasi-linear regions of gratings dips, was used to illuminate the sensor and observe the transmitted power. The power transmitted at both wavelengths was then fed to a matrix calculation to resolve temperature and torsional twist.

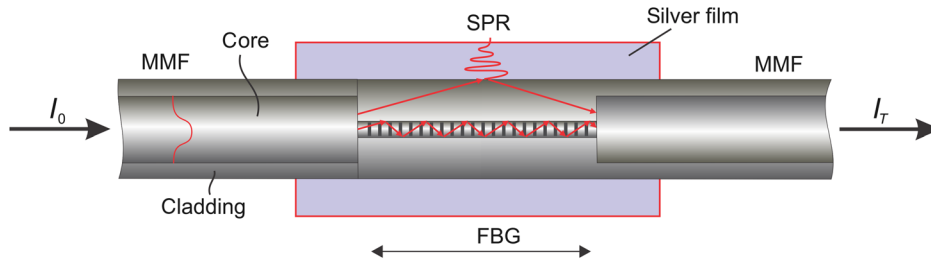


Fig. 44 RI and temperature sensor based on SPR by coupling light into the cladding.

2.9 Multiparameter Sensor Based on Surface Plasmon Resonance

Surface plasmon resonance (SPR) occurs when an incident light wave excites oscillations of free electrons at the boundary between two materials, which possess opposite signs of real parts of their dielectric functions (most typical examples are metal-dielectric interfaces). Multiparameter fiber-based SPR sensors are usually built in a way to remove part of the fiber's cladding locally, or using D-fibers,^{153,154} by coupling light into the cladding^{155,156} as shown in Fig. 44, by fiber tapering, or using photonics crystal fibers (PCF)¹⁵⁷ with the goal to allow for local access to the optical field propagating along the fiber.

These field access regions (exposed parts of the waveguides) are then covered by a thin layer of usually noble metal (gold or silver). For the resonance to occur, the phase constant of the mode in the fiber must match the propagation constant of the surface plasmon. Since these matching conditions depend on the surrounding RI and wavelength, SPR sensors are, in essence, RI sensors that can be interrogated spectrally. Since SPR can provide very sensitive RI measurements, it is reasonable, if not even imperative, to combine SPR sensing with temperature sensing capability. Thus multiparameter SPR-based sensors are almost exclusively found as sensitive dual-parameter sensors for measurements of RI and temperature. SPR sensor sections are usually interrogated spectrally and combined with a temperature sensing function using one of the sensing principles described in one of the previous sections of this review.

2.10 Other Principles

There are various other optical principles that can be utilized for multiparameter sensor design and that are not covered by the aforementioned classification.

One of the earliest reports of multiparameter sensors is described in Ref. 158. Here, simultaneous strain and

temperature measurements were achieved by application of a combined fiber-modal interferometer and polarimeter, created within a section of an elliptical core fiber. Different responses were obtained for interferometer and polarimeter with respect to the strain and temperature, which allows for separation of both parameters. An application of a multicore fiber for multiparameter sensing is described in Ref. 159. A short section of four-core fiber inserted in-between two lead single-mode fibers (Fig. 45) was used to simultaneous measure strain, temperature, and RI.¹⁵⁹ Launching of light in the center of the cladding of four-core fiber creates a complex interference pattern, which modulates coupling of light into the output fiber. The output spectrum contains different spectral dips with different sensitivities to strain, RI, and temperature.

In addition, an FBG was also written in one of the lead SMF fibers. Proper processing of this complex output spectrum (using the matrix method) allows for separation of all three parameters. PCF can also serve as a basis for several multiparameter sensors. Lin et al.¹⁶⁰ described a sensor that simulates measurement of strain and temperature, where several holes of the fiber were infiltrated selectively by a liquid. Interference among multiple modes in a structure like this creates a spectral signature that allows for extraction of temperature and strain. Microfabricated photonics crystal structures placed on the fiber tip also provide means for multiparameter sensing. In Ref. 161, a photonics crystal is fabricated on silicon using the lithographic process, and then transferred onto the tip of an optical fiber. The complex spectral response is sensitive to both RI and temperature. Similarly, in Ref. 162, measuring resonant wavelengths of different modes of a luminescent semiconductor photonics crystal cavity placed on the tip of an optical fiber are proposed and demonstrated for simultaneous measurement of RI and temperature. Lin et al.^{163,164} described an interesting, grating like, approach, where, instead, periodically, weak in-fiber mirrors are dispersed randomly along a short section of fiber (e.g., random grating) by application of femtosecond

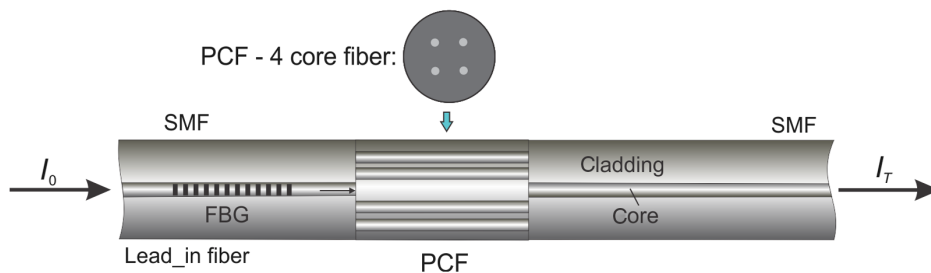


Fig. 45 Strain, temperature, and RI sensor.

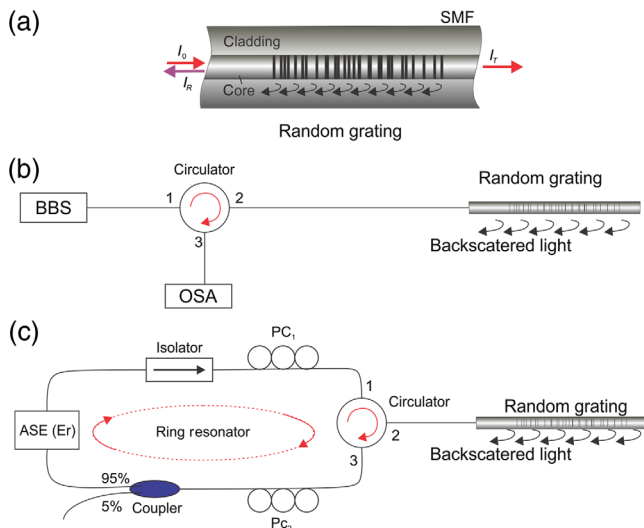


Fig. 46 (a) Random grating, (b) multiparameter sensor based on wavelength-division spectral cross correlation,¹⁶³ and (c) multiparameter sensor based on random fiber laser with random grating feedback.¹⁶⁴

laser inscription (Fig. 45). A broadband light source is launched into the fiber, while analyzing the back-reflected spectrum. The distinct interference fringes exhibited in the back-reflected spectrum are the result of both an MZI scheme via core-cladding mode coupling, and an FPI scheme via multiple reflected core-core mode couplings through reflections from numerous index-modified spots in the random grating. The external disturbances may cause changes in the interferometer length and effective refractive indices of the core mode and cladding modes in both types of created FPIs and MZIs. Such changes will, accordingly, result in a phase shift that leads to a spectral shift in the corresponding reflection spectrum. Temperature and RI measurements were demonstrated along such random grating (Fig. 46).

Fiber couplers and/or dual core fiber can also be employed in various RI sensing applications. When properly configured, they can be used to measure RI, RI-related parameters, and temperature. An example of combined temperature-magnetic field sensor (utilizing magneto-optic liquid that changes RI as a function of the B-field) was described in Ref. 165. In a similar way, simultaneous measurement of temperature and strain was also reported in Ref. 166. Here a dual-core plastic fiber was tapered to create a coupling zone.

Microknots and fiber microresonators also proved to be a basis for the creation of compact RI sensing devices. A possible approach for a dual-parameter RI-temperature sensor, which is based on a microknot resonator, is present in Ref. 167.

3 Multiparameter Sensors According to Type and Number of Parameters

In Table 1, we provide a list of sensor types, together with combinations of parameters that were demonstrated successfully for multiparameter sensing. The number of solutions for dual-parameter sensing is significantly larger than solutions for three or more parameters' sensing. Among dual-parameter sensors, sensors for simultaneous sensing of RI and temperature stand out in the number of reported

operational principles and sensing approaches. The number of reports on a three-parameter sensor is already significantly limited, whereas the number of reports for simultaneous sensing of four parameters' sensors reduces to about one example. It is more than apparent that combining more than two parameters represents a significant challenge.

4 Conclusion

This paper provided a review of work in the field of compact fiber-optic sensors that allow independent and simultaneous measurements of two or more different parameters. Sensor designs and corresponding signal processing schemes were reviewed and compared. Early work in this area can be traced back for over 25 years, but only recently this has attracted more in-depth research. This is probably a consequence of both increasing demands for multiparameter sensors in the field, and also recent developments of spectrally resolved signal interrogators that provide more versatile approaches to fiber-optic sensing and signal interrogation and interpretation. The majority of current work is focused into two-parameter sensors, where sensors for simultaneous sensing temperature and RI stand out in a number of recent publications. In dual-parameter sensors, temperature is the most frequently addressed parameter, i.e., a significant percentage of dual-parameter sensors is reported as sensors for measurements of particular parameters and temperature. While this is a consequence of actual needs in the field, temperature can also be measured in a number of different ways, which simplifies the design of sensors that combine temperature and any other parameter. The number of reported solutions for sensors that can sense three parameters simultaneously is, however, already limited, while sensors for sensing of parameters beyond three are very rare. Researching and engineering sensors capable of sensing three or more parameters will continue to present a challenge. This is probably related to difficulties in combining very different sensing principles into a single-sensor structure, while being able to resolve individual parameters independently one from another with low crosstalk.

In the future, we can expect further sensor miniaturization and integration of different sensor principles, with opportunities to sense more diversified sets of parameters. It can also be expected that both micromachining technologies and signal processing algorithms will improve, both in cost and performance, and will be further optimized to allow for more reliable multiparameter sensing. Some of these steps/challenges also need to be taken up by interrogator designers and producers. For example, spectral interrogator vendors could easily upgrade firmware in existing spectral interrogators to accommodate multiparameter sensor applications better (e.g., by adding on board IDFT with phase tracking algorithms and matrix calculation capabilities). We also need to warn on “overuse” of the matrix method, which is deeply anchored in existing multiparameter sensor designs. The matrix method assumes linear relationships among sensed optical and measured output parameters. These relationships are, however, often nonlinear, or they exhibit linear behavior only in limited ranges, while the matrix coefficients are often obtained by (two point) calibration. This might be quite a challenge in the design of commercial multiparameter sensors. Thus sensor designs that can provide “purer” relationships between actually measured optical parameters and

Table 1 An overview of multiparameter sensor types and corresponding principles of operation.

No. of parameters	Combinations of measuring parameters	FPI	MZI	MZI/MI and FPI	FBG	LPFBG	FBG and LPFBG	FBG/LPFBG and FPIs	FBG and MZI/MI	Fiber loop	Intensity-based	SPR	Other principle
Dual-parameter sensors	Pressure and temperature	3-7 and 10-12	41	62-67	51	90, 91, and 101							
	Pressure and RI	2											
	RI and temperature	15 and 16	19-21, 23, 24, 26, 27, 30, 31, 33-38, and 29	43-45	71-74	77-83	48-50	96-100	39, 102-118, and 120	130	1, 133-138, 140, 141, 144-146, 148, and 150	153-157	161-164 and 167
	Strain and temperature	1, 13, and 14	22 and 40	52-61 and 149	84	92-95	121 and 122	125-128	149	158, 160, and 166			
Three-p.s.	Relative humidity and temperature	17								129			
	Curvature/bending and temperature		25 and 28	76	85								
	Magnetic field and temperature			46									165
	Displacement and temperature			68-70			119				147		
	Strain and bending										142		
	Force and temperature			75	88								
	Rotation and displacement				86								
	Liquid level and temperature				87								
	Relative humidity and RI				47								
	Twist and temperature				89							152	
Four-p.s.	RI, strain, and temperature		32 and 42						117, 123, and 124		151		159
	Pressure, temperature, and RI											139 and 143	
	Torsion, strain, and temperature									131 and 132			
	Thermal conductivity, pressure, RI, and temperature	18											

sensed parameters, i.e., where the matrix method is not needed, or when at least some of the matrix coefficients go to zero, shall also probably be of high research interest. The latter might be of even greater interest when attempting to design usefully sensors for sensing of three or more parameters simultaneously. More rigorous metrological evaluation of multiparameter sensors/principles will be also needed in the future. Currently, the majority of published work is focused on demonstrating working principles with limited emphasis on achievable sensor performances. Parameters like resolution, crosstalk among measured parameters, and achievable absolute accuracy over sensors operating ranges will need to be analyzed systematically in detail, to make the proposed principles viable for field applications.

Finally, on the application side, there will be a question as to whether it is more economical to use more complex sensor structures combined with advanced algorithms, or rather rely on multiple individual sensors. Thus simplification of multiparameter sensor designs, sensor production technologies, designs that provide clear and simple relations between attainable optical parameters and measured parameters, and complexity of the calibration process that will guarantee sensor performance, will be detrimental for further commercial success of this technology. Work in this area is far from being completed.

Acknowledgments

We would like to thank the Slovenian Research Agency (ARRS) for supporting this work under Grant P2-0368 and P2-5494.

References

- Z. L. Ran et al., "Laser-machined cascaded micro cavities for simultaneous measurement of dual parameters under high temperature," *IEEE Sens. J.* **13**(5), 1988–1991 (2013).
- S. Pevac and D. Donlagić, "Miniature fiber-optic sensor for simultaneous measurement of pressure and refractive index," *Opt. Lett.* **39**(21), 6221–6224 (2014).
- J. D. Yin et al., "Batch-producible fiber-optic Fabry–Perot sensor for simultaneous pressure and temperature sensing," *IEEE Photonics Technol. Lett.* **26**(20), 2070–2073 (2014).
- Y. A. Zhang et al., "Simultaneous measurement of temperature and pressure with cascaded extrinsic Fabry–Perot interferometer and intrinsic Fabry–Perot interferometer sensors," *Opt. Eng.* **53**(6), 067101 (2014).
- B. Xu et al., "Fiber Fabry–Perot interferometer for measurement of gas pressure and temperature," *J. Lightwave Technol.* **34**(21), 4920–4925 (2016).
- Y. Z. Jiao et al., "Open-cavity Fabry–Perot interferometer pressure and temperature fiber sensor based on photonic crystal fiber," in *16th Int. Conf. Opt. Commun. Networks (ICOCN)* (2017).
- C. Pang et al., "MEMS Fabry–Perot sensor interrogated by optical system-on-a-chip for simultaneous pressure and temperature sensing," *Opt. Express* **21**(19), 21829–21839 (2013).
- T. H. Glisson, C. I. Black, and A. P. Sage, "Digital computation of discrete spectra using fast Fourier transform," *IEEE Trans. Audio Electroacoust.* **18**(3), 271–287 (1970).
- S. Mayrargue and T. Blu, "Relationship between high-resolution methods and discrete Fourier-transform," in *Int. Conf. Acoust., Speech, and Signal Process.*, Vols. 1–5, pp. 3321–3324 (1991).
- W. Z. Li, D. C. Abeyasinghe, and J. T. Boyd, "Multiplexed sensor system for simultaneous measurement of pressure and temperature," *Opt. Eng.* **43**(1), 148–156 (2004).
- S. Pevac and D. Donlagić, "Miniature all-fiber Fabry–Perot sensor for simultaneous measurement of pressure and temperature," *Appl. Opt.* **51**(19), 4536–4541 (2012).
- H. D. Bae et al., "Hybrid miniature Fabry–Perot sensor with dual optical cavities for simultaneous pressure and temperature measurements," *J. Lightwave Technol.* **32**(8), 1585–1593 (2014).
- H. Singh and J. S. Sirkis, "Simultaneously measuring temperature and strain using optical fiber microcavities," *J. Lightwave Technol.* **15**(4), 647–653 (1997).
- Y. Ouyang et al., "An in-fiber dual air-cavity Fabry–Perot interferometer for simultaneous measurement of strain and directional bend," *IEEE Sens. J.* **17**(11), 3362–3366 (2017).
- S. Pevac and D. Donlagić, "High resolution, all-fiber, micro-machined sensor for simultaneous measurement of refractive index and temperature," *Opt. Express* **22**(13), 16241–16253 (2014).
- S. Pevac and D. Donlagić, "Miniature fiber-optic Fabry–Perot refractive index sensor for gas sensing with a resolution of 5x10⁻⁹ RIU," *Opt. Express* **26**(18), 23868–23882 (2018).
- S. Pevac and D. Donlagić, "Miniature all-silica fiber-optic sensor for simultaneous measurement of relative humidity and temperature," *Opt. Lett.* **40**(23), 5646–5649 (2015).
- S. Pevac and D. Donlagić, "MultiParameter fiber-optic sensor for simultaneous measurement of thermal conductivity, pressure, refractive index, and temperature," *IEEE Photonics J.* **9**(1), 1–14 (2017).
- Y. F. Chen et al., "A hybrid multimode interference structure-based refractive index and temperature Fiber Sensor," *IEEE Sens. J.* **16**(2), 331–335 (2016).
- H. P. Luo et al., "Microfiber-based inline Mach–Zehnder interferometer for dual-parameter measurement," *IEEE Photonics J.* **7**(2), 1–8 (2015).
- Z. R. Tong et al., "Simultaneous measurement based on composite interference structure," *IEEE Photonics Technol. Lett.* **26**(13), 1310–1313 (2014).
- Q. Wu et al., "Fibre heterostructure for simultaneous strain and temperature measurement," *Electron. Lett.* **47**(12), 713–714 (2011).
- R. Xiong et al., "Simultaneous measurement of refractive index and temperature based on modal interference," *IEEE Sens. J.* **14**(8), 2524–2528 (2014).
- J. M. Zhang et al., "Refractive index and temperature sensors based on no-core fiber cascaded with long period fiber grating," *J. Mod. Opt.* **65**(9), 1098–1103 (2018).
- Y. X. Zhang et al., "Simultaneous measurement of temperature and curvature based on hollow annular core fiber," *IEEE Photonics Technol. Lett.* **26**(11), 1128–1131 (2014).
- Y. H. Hu et al., "Simultaneous measurement of refractive index and temperature based on a core-offset Mach–Zehnder interferometer," in *16th Int. Conf. Opt. Commun. Networks (ICOCN)* (2017).
- H. J. Kim and Y. G. Han, "Polarization-dependent in-line Mach–Zehnder interferometer for discrimination of temperature and ambient index sensitivities," *J. Lightwave Technol.* **30**(8), 1037–1041 (2012).
- Y. Zhao, L. Cai, and X. G. Li, "In-fiber modal interferometer for simultaneous measurement of curvature and temperature based on hollow core fiber," *Opt. Laser Technol.* **92**, 138–141 (2017).
- Y. Li et al., "Double-pass in-line fiber taper Mach–Zehnder interferometer sensor," *IEEE Photonics Technol. Lett.* **22**(23), 1750–1752 (2010).
- J. B. Liu, D. N. Wang, and L. Zhang, "Slightly tapered optical fiber with dual inner air-cavities for simultaneous refractive index and temperature measurement," *J. Lightwave Technol.* **34**(21), 4872–4876 (2016).
- X. Q. Ni et al., "A hybrid Mach–Zehnder interferometer for refractive index and temperature measurement," *IEEE Photonics Technol. Lett.* **28**(17), 1850–1853 (2016).
- J. Harris et al., "Highly sensitive in-fiber interferometric refractometer with temperature and axial strain compensation," *Opt. Express* **21**(8), 9996–10009 (2013).
- C. R. Liao, H. F. Chen, and D. N. Wang, "Ultracompact optical fiber sensor for refractive index and high-temperature measurement," *J. Lightwave Technol.* **32**(14), 2531–2535 (2014).
- J. Su et al., "Double-parameters optical fiber sensor based on spherical structure and multimode fiber," *IEEE Photonics Technol. Lett.* **27**(4), 427–430 (2015).
- H. H. Wang et al., "Simultaneous measurement of refractive index and temperature based on asymmetric structures modal interference," *Opt. Commun.* **364**, 191–194 (2016).
- L. Zhang et al., "Simultaneous refractive index and temperature sensing with precise sensing location," *IEEE Photonics Technol. Lett.* **28**(8), 891–894 (2016).
- R. A. Zhao et al., "Polarization-maintaining fiber sensor for simultaneous measurement of the temperature and refractive index," *Opt. Eng.* **56**(5), 057113 (2017).
- A. P. Zhang et al., "Sandwiched long-period gratings for simultaneous measurement of refractive index and temperature," *IEEE Photonics Technol. Lett.* **17**(11), 2397–2399 (2005).
- M. L. Xiong et al., "Simultaneous refractive index and temperature measurement based on Mach–Zehnder interferometer concatenating two Bi-tapers and a long-period grating," *IEEE Sens. J.* **16**(11), 4295–4299 (2016).
- J. C. Bian et al., "A polarization maintaining fiber sensor for simultaneous measurement of temperature and strain," *Optik* **127**(20), 10090–10095 (2016).
- W. J. Bock and T. A. Eftimov, "Simultaneous hydrostatic-pressure and temperature-measurement employing an Lp(01)-Lp(11) fiber optic polarization-sensitive intermodal interferometer," *IEEE Trans. Instrum. Meas.* **43**(2), 337–340 (1994).

42. N. Zhang et al., "Simultaneous measurement of refractive index, strain and temperature using a tapered structure based on SMF," *Opt. Commun.* **410**, 70–74 (2018).
43. D. W. Kim et al., "Simultaneous measurement of refractive index and temperature based on a reflection-mode long-period grating and an intrinsic Fabry–Perot interferometer sensor," *Opt. Lett.* **30**(22), 3000–3002 (2005).
44. Y. Zhao et al., "Measurement of RI and temperature using composite interferometer with hollow-core fiber and photonic crystal fiber," *IEEE Trans. Instrum. Meas.* **65**(11), 2631–2636 (2016).
45. H. Sun et al., "A hybrid fiber interferometer for simultaneous refractive index and temperature measurements based on Fabry–Perot/Michelson interference," *IEEE Sens. J.* **13**(5), 2039–2044 (2013).
46. X. G. Li et al., "Measurement of magnetic field and temperature based on fiber-optic composite interferometer," *IEEE Trans. Instrum. Meas.* **66**(7), 1906–1911 (2017).
47. L. Alwis, T. Sun, and K. T. V. Grattan, "Temperature-compensated optimized relative humidity and refractive index sensors using a hybrid fibre grating configuration," in *IEEE SENSORS*, pp. 1367–1368 (2015).
48. C. Berrettoni et al., "Fibre tip sensor with embedded FBG-LPG for temperature and refractive index determination by means of the simple measurement of the FBG characteristics," *J. Sens.* **20**, 491391 (2015).
49. X. F. Chen et al., "Optical sensor based on hybrid LPG/FBG in D-fiber for simultaneous refractive index and temperature measurement," *Proc. SPIE* **5634**, 140–145 (2004).
50. D. A. C. Enriquez, A. R. da Cruz, and T. M. R. Giraldo, "Hybrid FBG-LPG sensor for surrounding refractive index and temperature simultaneous discrimination," *Opt. Laser Technol.* **44**(4), 981–986 (2012).
51. Y. L. Wang et al., "Simultaneous temperature and pressure measurement using a packaged FBG and LPG," in *15th Optoelectron. and Commun. Conf. (OECC)*, pp. 814–815 (2010).
52. R. Aashia and S. Asokan, "Simultaneous measurement of strain and temperature using type I and pre-strained fiber Bragg gratings," in *IEEE SENSORS*, Vols. 1–3, pp. 1229–1231 (2009).
53. P. M. Cavaleiro et al., "Simultaneous measurement of strain and temperature using Bragg gratings written in germanosilicate and boron-codoped germanosilicate fibers," *IEEE Photonics Technol. Lett.* **11**(12), 1635–1637 (1999).
54. O. Frazao and J. L. Santos, "Simultaneous measurement of strain and temperature using a Bragg grating structure written in germanosilicate fibres," *J. Opt. A Pure Appl. Opt.* **6**(6), 553–556 (2004).
55. Y. G. Han et al., "Multiwavelength Raman-fiber-laser-based long-distance remote sensor for simultaneous measurement of strain and temperature," *Opt. Lett.* **30**(11), 1282–1284 (2005).
56. Y. L. Lo, "Using in-fiber Bragg-grating sensors for measuring axial strain and temperature simultaneously on surfaces of structures," *Opt. Eng.* **37**(8), 2272–2276 (1998).
57. Y. L. Lo and J. S. Sirkis, "Simple method to measure temperature and axial strain simultaneously using one in-fiber Bragg-grating sensor," *Proc. SPIE* **3042**, 237–246 (1997).
58. S. K. Mondal et al., "Embedded dual fiber Bragg grating sensor for simultaneous measurement of temperature and load (strain) with enhanced sensitivity," *Microwave Opt. Technol. Lett.* **51**(7), 1621–1624 (2009).
59. R. Rajinikumar et al., "Fiber Bragg grating sensors for measuring temperature and strain simultaneously at cryogenic temperature," *AIP Conf. Proc.* **985**, 383–390 (2008).
60. Z. Wenjun et al., "A novel FBG sensing head geometry for strain-temperature discrimination," in *Asia Commun. and Photonics Conf. and Exhib.*, Shanghai, China (2009).
61. W. L. Liu, W. Z. Li, and J. P. Yao, "Real-time interrogation of a linearly chirped fiber Bragg grating sensor for simultaneous measurement of strain and temperature," *IEEE Photonics Technol. Lett.* **23**(18), 1340–1342 (2011).
62. Y. Q. Liu et al., "Simultaneous pressure and temperature measurement with polymer-coated fibre Bragg grating," *Electron. Lett.* **36**(6), 564–566 (2000).
63. X. G. Qiao and M. Fiddy, "Distributed optical fiber Bragg grating sensor for simultaneous measurement of pressure and temperature in the oil and gas downhole," *Proc. SPIE* **4870**, 554–558 (2002).
64. Y. Zhao, Y. B. Liao, and S. R. Lai, "Simultaneous measurement of down-hole high pressure and temperature with a bulk-modulus and FBG sensor," *IEEE Photonics Technol. Lett.* **14**(11), 1584–1586 (2002).
65. C. M. Lin et al., "High-sensitivity simultaneous pressure and temperature sensor using a superstructure fiber grating," *IEEE Sens. J.* **6**(3), 691–696 (2006).
66. C. A. Wu, Y. Zhang, and B. O. Guan, "Simultaneous measurement of temperature and hydrostatic pressure using Bragg gratings in standard and grapefruit microstructured fibers," *IEEE Sens. J.* **11**(2), 489–492 (2011).
67. L. Htein et al., "Bragg grating in novel two-core holey fiber for simultaneous measurement of pressure and temperature," in *Opto-Electron. and Commun. Conf. (OECC) and Photonics Global Conf. (PGC)* (2017).
68. Y. L. Yu et al., "Fiber Bragg grating sensor for simultaneous measurement of displacement and temperature," *Opt. Lett.* **25**(16), 1141–1143 (2000).
69. W. G. Zhang et al., "FBG-type sensor for simultaneous measurement of force (or displacement) and temperature based on bilateral cantilever beam," *IEEE Photonics Technol. Lett.* **13**(12), 1340–1342 (2001).
70. S. C. Tao, X. P. Dong, and B. W. Lai, "A sensor for simultaneous measurement of displacement and temperature based on the Fabry–Perot Effect of a fiber Bragg grating," *IEEE Sens. J.* **17**(2), 261–266 (2017).
71. W. Ecke et al., "Optical fiber grating sensor network for monitoring refractive index and temperature distributions in fluids," *Proc. SPIE* **3783**, 176–183 (1999).
72. A. Iadicicco et al., "Nonuniform thinned fiber Bragg gratings for simultaneous refractive index and temperature measurements," *IEEE Photonics Technol. Lett.* **17**(7), 1495–1497 (2005).
73. Z. Chen et al., "Side polished fiber Bragg grating sensor for simultaneous measurement of refractive index and temperature," *Proc. SPIE* **7753**, 77538K (2011).
74. H. Z. Yang et al., "Cladless few mode fiber grating sensor for simultaneous refractive index and temperature measurement," *Sens. Actuators A* **228**, 62–68 (2015).
75. T. Guo et al., "FBG-type sensor for simultaneous measurement of temperature and force based on reflection spectrum broadening," *Proc. SPIE* **6019**, 60191T (2005).
76. Y. G. Han et al., "Simultaneous measurement of bending and temperature based on a single sampled chirped fiber Bragg grating embedded on a flexible cantilever beam," *Opt. Lett.* **31**(19), 2839–2841 (2006).
77. Q. Han et al., "Long-period grating inscribed on concatenated double-clad and single-clad fiber for simultaneous measurement of temperature and refractive index," *IEEE Photonics Technol. Lett.* **24**(13), 1130–1132 (2012).
78. J. H. Yan et al., "Simultaneous measurement of refractive index and temperature by using dual long-period gratings with an etching process," *IEEE Sens. J.* **7**(9–10), 1360–1361 (2007).
79. T. Zhu, Y. J. Rao, and Q. J. Mo, "Simultaneous measurement of refractive index and temperature using a single ultralong-period fiber grating," *IEEE Photonics Technol. Lett.* **17**(12), 2700–2702 (2005).
80. B. A. L. Gwandu et al., "Simultaneous refractive index and temperature measurement using cascaded long-period grating in double-cladding fibre," *Electron. Lett.* **38**(14), 695–696 (2002).
81. C. L. Zhao et al., "Simultaneous temperature and refractive index measurements using a 3 degrees slanted multimode fiber Bragg grating," *J. Lightwave Technol.* **24**(2), 879–883 (2006).
82. N. J. Alberto et al., "Simultaneous temperature and refractive index sensor based on a tilted fibre Bragg grating," *Proc. SPIE* **8001**, 800124 (2011).
83. A. C. L. Wong et al., "Simultaneous two-parameter sensing using a single tilted moire fiber Bragg grating with discrete wavelet transform technique," *IEEE Photonics Technol. Lett.* **22**(21), 1574–1576 (2010).
84. Y. Milao, B. Liu, and Q. Zhao, "Simultaneously measurement of strain and temperature using single tilted fibre Bragg grating," *Electron. Lett.* **44**(21), 1242–1243 (2008).
85. J. Sun et al., "Application of an artificial neural network for simultaneous measurement of bending curvature and temperature with long-period fiber gratings," *Sens. Actuators A* **137**(2), 262–267 (2007).
86. P. Kisala, D. Harasim, and J. Mroczka, "Temperature-insensitive simultaneous rotation and displacement (bending) sensor based on tilted fiber Bragg grating," *Opt. Express* **24**(26), 29922–29929 (2016).
87. T. Osuch et al., "Simultaneous measurement of liquid level and temperature using tilted fiber Bragg grating," *IEEE Sens. J.* **16**(5), 1205–1209 (2016).
88. J. B. Xu et al., "Simultaneous force and temperature measurement using long-period grating written on the joint of a microstructured optical fiber and a single mode fiber," *Appl. Opt.* **49**(3), 492–496 (2010).
89. Y. Yongqin et al., "An in-line fiber-optic modal interferometer for simultaneous measurement of twist and ambient temperature," *Sens. Bio-Sens. Res.* **2**, 38–42 (2014).
90. M. M. Ali et al., "PCF-cavity FBG Fabry–Perot resonator for simultaneous measurement of pressure and temperature," *IEEE Sens. J.* **15**(12), 6921–6925 (2015).
91. S. N. Wu et al., "FBG incorporated side-open Fabry–Perot cavity for simultaneous gas pressure and temperature measurements," *J. Lightwave Technol.* **34**(16), 3761–3767 (2016).
92. W. C. Du, X. M. Tao, and H. Y. Tam, "Fiber Bragg grating cavity sensor for simultaneous measurement of strain and temperature," *IEEE Photonics Technol. Lett.* **11**(1), 105–107 (1999).
93. X. D. Jin, J. S. Sirkis, and J. K. Chung, "Optical fiber sensor for simultaneous measurement of strain and temperature," *Proc. SPIE* **3042**, 120–127 (1997).
94. Q. Liu et al., "Highly integrated FP/FBG sensor for simultaneous measurement of high temperature and strain," *IEEE Photonics Technol. Lett.* **26**(17), 1715–1717 (2014).
95. Y. J. Rao et al., "Hybrid LPPG/MEFPI sensor for simultaneous measurement of high-temperature and strain," *Opt. Express* **15**(22), 14936–14941 (2007).
96. C. Gouveia et al., "Fabry–Perot cavity based on a high-birefringent fiber Bragg grating for refractive index and temperature measurement," *IEEE Sens. J.* **12**(1), 17–21 (2012).

97. Y. G. Liu et al., "Micro-structured optical fiber sensor for simultaneous measurement of temperature and refractive index," *Opt. Fiber Technol.* **41**, 168–172 (2018).
98. J. J. Zhang et al., "Microfiber Fabry–Perot interferometer for dual-parameter sensing," *J. Lightwave Technol.* **31**(10), 1608–1615 (2013).
99. Y. Xiang et al., "Quasi-distributed dual-parameter optical fiber sensor based on cascaded microfiber Fabry–Perot interferometers," *IEEE Photonics J.* **10**(2), 1–9 (2018).
100. Y. Xiang et al., "Distributed dual-parameter optical fiber sensor based on cascaded microfiber Fabry–Perot Interferometers," in *25th Int. Conf. Opt. Fiber Sens. (OFS)* (2017).
101. K. Bremer et al., "Feedback stabilized interrogation technique for EFPI/FBG hybrid fiber-optic pressure and temperature sensors," *IEEE Sens. J.* **12**(1), 133–138 (2012).
102. F. Ahmed et al., "Bragg grating embedded in Mach–Zehnder interferometer for refractive index and temperature sensing," *IEEE Photonics Technol. Lett.* **28**(18), 1968–1971 (2016).
103. Y. Cao, C. Zhao, and Z. R. Tong, "All fiber sensor based on Mach–Zehnder interferometer for simultaneous measurement of temperature and refractive index," *Optoelectron. Lett.* **11**(6), 438–443 (2015).
104. C. R. Liao et al., "Fiber in-line Mach–Zehnder interferometer embedded in FBG for simultaneous refractive index and temperature measurement," *IEEE Photonics Technol. Lett.* **22**(22), 1686–1688 (2010).
105. Y. F. Lu et al., "Refractive index and temperature sensor based on double-pass M-Z interferometer with an FBG," *IEEE Photonics Technol. Lett.* **26**(11), 1124–1127 (2014).
106. Q. Q. Yao et al., "Simultaneous measurement of refractive index and temperature based on a core-offset Mach–Zehnder interferometer combined with a fiber Bragg grating," *Sens. Actuators A* **209**, 73–77 (2014).
107. M. H. Zhou, X. Y. Dong, and X. H. Liu, "Simultaneous measurement of temperature and refractive index with thin-core fiber MZI containing fiber Bragg grating," in *16th Int. Conf. Opt. Commun. Networks (ICOCN)* (2017).
108. L. C. Li et al., "Novel NCF-FBG interferometer for simultaneous measurement of refractive index and temperature," *IEEE Photonics Technol. Lett.* **24**(24), 2268–2271 (2012).
109. X. J. Yu et al., "In-fiber modal interferometer for simultaneous measurement of refractive index and temperature," *IEEE Photonics Technol. Lett.* **28**(2), 189–192 (2016).
110. C. Zhang et al., "Multipoint refractive index and temperature fiber optic sensor based on cascaded no core fiber–fiber Bragg grating structures," *Opt. Eng.* **56**(2), 027102 (2017).
111. Y. L. Bai et al., "Simultaneous measurement of refractive index and temperature based on NFN structure," *IEEE Photonics Technol. Lett.* **26**(21), 2193–2196 (2014).
112. Y. Cao et al., "Simultaneous measurement of temperature and refractive index based on a core-offset Mach–Zehnder interferometer cascaded with a long-period fiber grating," *Optoelectron. Lett.* **11**(1), 69–72 (2015).
113. J. L. Li et al., "Long-period fiber grating cascaded to an S fiber taper for simultaneous measurement of temperature and refractive index," *IEEE Photonics Technol. Lett.* **25**(9), 888–891 (2013).
114. S. Yang et al., "Refractive index and temperature sensor based on cladding-mode Bragg grating excited by abrupt taper interferometer," *Chin. Opt. Lett.* **11**(12), 120604–120607 (2013).
115. Q. Q. Yao et al., "A sandwich fiber sensor for simultaneous measurement of RI and temperature," in *16th Int. Conf. Opt. Commun. Networks (ICOCN)* (2017).
116. X. P. Zhang et al., "Core-offset-based fiber Bragg grating sensor for refractive index and temperature measurement," *Opt. Eng.* **52**(2), 024402 (2013).
117. S. M. Lee, S. S. Saini, and M. Y. Jeong, "Simultaneous measurement of refractive index, temperature, and strain using etched-core fiber Bragg grating sensors," *IEEE Photonics Technol. Lett.* **22**(19), 1431–1433 (2010).
118. T. G. Liu et al., "Sensor based on macrobent fiber Bragg grating structure for simultaneous measurement of refractive index and temperature," *Appl. Opt.* **55**(4), 791–795 (2016).
119. K. Tian et al., "Simultaneous measurement of displacement and temperature based on a balloon-shaped bent SMF Structure incorporating an LPG," *J. Lightwave Technol.* **36**(20), 4960–4966 (2018).
120. G. L. Yin et al., "Simultaneous refractive index and temperature measurement with LPFG and liquid-filled PCF," *IEEE Photonics Technol. Lett.* **27**(4), 375–378 (2015).
121. M. J. Kim et al., "Simultaneous measurement of temperature and strain based on double cladding fiber interferometer assisted by fiber grating pair," *IEEE Photonics Technol. Lett.* **20**(13–16), 1290–1292 (2008).
122. B. Dong et al., "Simultaneous strain and temperature measurement using a compact photonic crystal fiber inter-modal interferometer and a fiber Bragg grating," *Appl. Opt.* **49**(32), 6232–6235 (2010).
123. Y. J. Jiang et al., "Multi-parameter sensing using a Fiber Bragg grating inscribed in dual-mode fiber," *IEEE Photonics Technol. Lett.* **29**(19), 1607–1610 (2017).
124. R. Oliveira et al., "Simultaneous measurement of strain, temperature and refractive index based on multimode interference, fiber tapering and fiber Bragg gratings," *Meas. Sci. Technol.* **27**(7), 075107 (2016).
125. G. Y. Sun, D. S. Moon, and Y. Chung, "Simultaneous temperature and strain measurement using two types of high-birefringence fibers in Sagnac loop mirror," *IEEE Photonics Technol. Lett.* **19**(21–24), 2027–2029 (2007).
126. O. Frazao et al., "Strain and temperature discrimination using high-birefringence erbium-doped fiber loop mirror with high pump power laser," *IEEE Photonics Technol. Lett.* **20**(9–12), 1033–1035 (2008).
127. Y. G. Han, Y. Chung, and S. B. Lee, "Discrimination of strain and temperature based on a polarization-maintaining photonic crystal fiber incorporating an erbium-doped fiber," *Opt. Commun.* **282**(11), 2161–2164 (2009).
128. Q. Wang et al., "Simultaneous measurement of strain and temperature with polarization maintaining Fiber Bragg grating loop mirror," *Instrum. Sci. Technol.* **42**(3), 298–307 (2014).
129. H. L. Liu et al., "Simultaneous measurement of humidity and temperature based on a long-period fiber grating inscribed in fiber loop mirror," *IEEE Sens. J.* **14**(3), 893–896 (2014).
130. Y. N. Zhang et al., "Simultaneous measurement of hydrogen concentration and temperature based on fiber loop mirror combined with PCF," *IEEE Sens. J.* **18**(6), 2369–2376 (2018).
131. X. Wang et al., "Simultaneous measurement of torsion, strain and temperature using a side-leakage photonic crystal fiber loop mirror," *Infrared Phys. Technol.* **76**, 603–607 (2016).
132. O. Frazao et al., "Simultaneous measurement of multiparameters using a Sagnac interferometer with polarization maintaining side-hole fiber," *Appl. Opt.* **47**(27), 4841–4848 (2008).
133. A. C. L. Wong et al., "Composite structure distributed Bragg reflector fiber laser for simultaneous two-parameter sensing," *IEEE Photonics Technol. Lett.* **22**(19), 1464–1466 (2010).
134. H. Y. Choi et al., "Cross-talk free and ultra-compact fiber optic sensor for simultaneous measurement of temperature and refractive index," *Opt. Express* **18**(1), 141–149 (2010).
135. T. T. Wang and M. Wang, "Fabry–Perot fiber sensor for simultaneous measurement of refractive index and temperature based on an in-fiber ellipsoidal cavity," *IEEE Photonics Technol. Lett.* **24**(19), 1733–1736 (2012).
136. M. W. Yang, D. N. Wang, and C. R. Liao, "Fiber Bragg grating with micro-holes for simultaneous and independent refractive index and temperature sensing," *IEEE Photonics Technol. Lett.* **23**(20), 1511–1513 (2011).
137. H. Y. Meng et al., "Fiber Bragg grating-based fiber sensor for simultaneous measurement of refractive index and temperature," *Sens. Actuators B* **150**(1), 226–229 (2010).
138. M. Li et al., "Fiber-optic sensor tip for measuring temperature and liquid refractive index," *Opt. Eng.* **53**(11), 116110 (2014).
139. R. D. Pechstedt, "Fibre optical sensor for simultaneous measurement of pressure, temperature and refractive index," *Proc. SPIE* **9157**, 91570I (2014).
140. Y. Zhao, L. Cai, and X. G. Li, "High sensitive modal interferometer for temperature and refractive index measurement," *IEEE Photonics Technol. Lett.* **27**(12), 1341–1344 (2015).
141. X. Y. Zhang et al., "Miniature end-capped fiber sensor for refractive index and temperature measurement," *IEEE Photonics Technol. Lett.* **26**(1), 7–10 (2014).
142. A. Sun and Z. S. Wu, "Multimode interference in single mode-multimode FBG for simultaneous measurement of strain and bending," *IEEE Sens. J.* **15**(6), 3390–3394 (2015).
143. K. Bremer et al., "Pressure, temperature and refractive index determination of fluids using a single fibre optic point sensor," *Sens. Actuators A* **256**, 84–88 (2017).
144. F. F. Shi et al., "Simultaneous measurement of refractive index and temperature base on three-beam interferometric fiber-optic," in *Optoelectron. Global Conf. (OGC)* (2015).
145. O. R. R. Naeini, H. Latifi, and M. I. Zibaii, "Simultaneous measurement of refractive index and temperature with micro silica sphere cavity hybrid Fabry–Perot optical fiber sensor," *Proc. SPIE* **9634**, 963472 (2015).
146. H. C. Xue et al., "Single-mode-multimode fiber structure based sensor for simultaneous measurement of refractive index and temperature," *IEEE Sens. J.* **13**(11), 4220–4223 (2013).
147. Y. T. Chang et al., "Using a fiber loop and fiber Bragg grating as a fiber optic sensor to simultaneously measure temperature and displacement," *Sensors* **13**(5), 6542–6551 (2013).
148. X. L. Tan et al., "UV-curable polymer microhemisphere-based fiber-optic Fabry–Perot interferometer for simultaneous measurement of refractive index and temperature," *IEEE Photonics J.* **6**(4), 1–8 (2014).
149. J. Jung, N. Park, and B. Lee, "Simultaneous measurement of strain and temperature by use of a single fiber Bragg grating written in an erbium:ytterbium-doped fiber," *Appl. Opt.* **39**(7), 1118–1120 (2000).
150. J. Zhang et al., "Simultaneous measurement of refractive index and temperature using a Michelson fiber interferometer with a hi-bi fiber probe," *IEEE Sens. J.* **13**(6), 2061–2065 (2013).

151. N. J. Alberto et al., "Three-parameter optical fiber sensor based on a tilted fiber Bragg grating," *Appl. Opt.* **49**(31), 6085–6091 (2010).
152. L. L. Xian, P. Wang, and H. P. Li, "Power-interrogated and simultaneous measurement of temperature and torsion using paired helical long-period fiber gratings with opposite helicities," *Opt. Express* **22**(17), 20260–20267 (2014).
153. S. J. Weng et al., "Double-side polished fiber SPR sensor for simultaneous temperature and refractive index measurement," *IEEE Photonics Technol. Lett.* **28**(18), 1916–1919 (2016).
154. D. F. Santos, A. Guerreiro, and J. M. Baptista, "Simultaneous plasmonic measurement of refractive index and temperature based on a D-type fiber sensor with gold wires," *IEEE Sens. J.* **17**(8), 2439–2446 (2017).
155. T. Hu, Y. Zhao, and A. N. Song, "Fiber optic SPR sensor for refractive index and temperature measurement based on MMF-FBG-MMF structure," *Sens. Actuators B* **237**, 521–525 (2016).
156. J. S. Velazquez-Gonzalez et al., "Simultaneous measurement of refractive index and temperature using a SPR-based fiber optic sensor," *Sens. Actuators B* **242**, 912–920 (2017).
157. N. N. Luan, C. F. Ding, and J. Q. Yao, "A refractive index and temperature sensor based on surface plasmon resonance in an exposed-core microstructured optical fiber," *IEEE Photonics J.* **8**(2), 1–8 (2016).
158. A. M. Vengsarkar et al., "Fiber optic dual-technique sensor for simultaneous measurement of strain and temperature," *J. Lightwave Technol.* **12**(1), 170–177 (1994).
159. C. Li et al., "Simultaneous measurement of refractive index, strain, and temperature based on a four-core fiber combined with a fiber Bragg grating," *Opt. Laser Technol.* **90**, 179–184 (2017).
160. C. P. Lin et al., "Photonic crystal fiber with selective infiltration for high sensitivity simultaneous temperature and strain measurement," in *Conf. Lasers and Electro-Opt. Pacific Rim (CLEO-PR)* (2017).
161. I. W. Jung et al., "Highly sensitive monolithic silicon photonic crystal fiber tip sensor for simultaneous measurement of refractive index and temperature," *J. Lightwave Technol.* **29**(9), 1367–1374 (2011).
162. M. Boerkamp et al., "Multiple modes of a photonic crystal cavity on a fiber tip for multiple parameter sensing," *J. Lightwave Technol.* **33**(18), 3901–3906 (2015).
163. Y. P. Xu et al., "Optical fiber random grating-based multiparameter sensor," *Opt. Lett.* **40**(23), 5514–5517 (2015).
164. Y. P. Xu et al., "Multi-parameter sensor based on random fiber lasers," *AIP Adv.* **6**(9), 095009 (2016).
165. F. F. Wei et al., "Simultaneous measurement of both magnetic field strength and temperature with a microfiber coupler based fiber laser sensor," in *25th Int. Conf. Opt. Fiber Sens. (OFS)* (2017).
166. S. Gao et al., "Simultaneous measurement of temperature and strain in a dual-core As₂Se₃-PMMA taper," *IEEE Photonics Technol. Lett.* **30**(1), 79–82 (2018).
167. A. D. Gomes and O. Frazao, "Microfiber knot with taper interferometer for temperature and refractive index discrimination," *IEEE Photonics Technol. Lett.* **29**(18), 1517–1520 (2017).

Simon Pevce is an assistant professor at the University of Maribor. He has a broad background in the fields of photonics systems, optical fiber sensors, and micro-opto-electro-mechanical systems (MOEMS). His main experiences and knowledge have been acquired in the Laboratory for Electro-Optics and Sensor Systems, where he mostly works on developing technology for micromachining of optical fibers, including selective etching, to produce/develop all kinds of miniature all-fiber Fabry–Perot sensors. His bibliography currently comprises 5 U.S. patents and 11 scientific articles in high-ranking journals.

Denis Donlagić is a full professor at the University of Maribor. He has a broad background in the fields of photonics systems, opto-electronics systems, optical fibers, and MOEMS. In particular, he has research and development experience in the fields of optical fiber sensors, optical fibers, and opto-electronics system design. His focus is in finding new scientific paradigms and technology concepts, while bringing them into practical applications. His bibliography currently comprises 16 U.S. patents and 60 scientific articles in high-ranking journals.